VYSOKÉ UČENÍ TECHNICKÉ V BRNĚ

BRNO UNIVERSITY OF TECHNOLOGY

FAKULTA STROJNÍHO INŽENÝRSTVÍ

FACULTY OF MECHANICAL ENGINEERING

ÚSTAV MECHANIKY TĚLES, MECHATRONIKY A BIOMECHANIKY

INSTITUTE OF SOLID MECHANICS, MECHATRONICS AND BIOMECHANICS

ANALÝZA KOEFICIENTU TŘENÍ OBTOKOVÉHO VENTILU TURBODMYCHADLA

FRICTION COEFFICIENT ANALYSIS OF THE TURBOCHARGER BYPASS VALVE

DIPLOMOVÁ PRÁCE

MASTER'S THESIS

AUTOR PRÁCE — **Bc. JURAJ WOLF**

AUTHOR

VEDOUCÍ PRÁCE — **Ing. PETR KREJČÍ, Ph.D.**

SUPERVISOR

BRNO 2019

VYSOKÉ UČENÍ TECHNICKÉ V BRNĚ
FAKULTA STROJNÍHO INŽENÝRSTVÍ

Zadání diplomové práce

Ústav:	Ústav mechaniky těles, mechatroniky a biomechaniky
Student:	**Bc. Juraj Wolf**
Studijní program:	Aplikované vědy v inženýrství
Studijní obor:	Mechatronika
Vedoucí práce:	**Ing. Petr Krejčí, Ph.D.**
Akademický rok:	2018/19

Ředitel ústavu Vám v souladu se zákonem č.111/1998 o vysokých školách a se Studijním a zkušebním řádem VUT v Brně určuje následující téma diplomové práce:

Analýza koeficientu tření obtokového ventilu turbodmychadla

Stručná charakteristika problematiky úkolu:

Návrh aktuátoru pro danou aplikaci turbodmychadla závisí na tření v kinematických členech. Nejvíce ke tření přispívá kontakt mezi pouzdrem a hřídelí obtokového ventilu turbodmychadla. Velikost tření závisí na různych parametrech, jako je například geometrie obtokového ventilu, způsob výroby materiálu, drsnosti povrchu, teplota, atd. Účelem této práce je určení koeficientu tření pro různé návrhové parametry obtokového ventilu turbodmychadla.

Cíle diplomové práce:

Navrhněte upínací zařízení pro testovaní obtokového ventilu na stolici pro měření průtoku.
Proveďte CFD simulaci obtokového ventilu při statickém aerodynamickém zatížení.
Vytvořte analytický model kinematiky systému obtokového ventilu se třením.
Experimentálně změřte sílu v táhle kinematického řetězce při daných okrajových podmínkách.
Porovnejte průběh síly z experimentu s analytickým řešením.
Vyjádřete závislost koeficientu tření na různých parametrech obtokového ventilu.

Seznam doporučené literatury:

FIGLIOLA Richard S., BEASLEY Donald E.: Theory and design for Mechanical Measurement, 2nd. ed., John Wiley and Sons, Inc., USA 1995

WHEELER Anthony J., GANJI Ahmad R.: Introduction to Engineering Experimentation, Prentice Hall, Upper Saddle River, New Jersey 07458, USA 1996

Termín odevzdání diplomové práce je stanoven časovým plánem akademického roku 2018/19

V Brně, dne

L. S.

prof. Ing. Jindřich Petruška, CSc. ředitel ústavu	doc. Ing. Jaroslav Katolický, Ph.D. děkan fakulty

Abstrakt
Cílem této diplomové práce je představit novou metodu určení koeficientu tření obtokového ventilu turbodmychadla. Za tímto účelem bylo navrhnuto a zkonstruováno testovací zařízení. Vysledky z testů byli zpracovány a porovnany v simulačních programech ANSYS a MSC Adams. Predstavená metoda poskytuje presné a dostapuné meření koeficientu tření pro ruzne typy obtokového ventilu turbodmychadla.

Summary
Aim of the diploma thesis is set to present a new method for evaluation of the friction coefficient of the wastegate valve system. A test fixture was designed and manufactured for this purpose. Simulations in ANSYS and MSC Adams support test results. The developed method provides an accurate and affordable solution for investigating of friction coefficient for various valves of turbochargers wastegate.

Klíčová slova
CFD, Adams, Tření, Koeficient tření, Turbodmychadlo, Obtokový ventil

Keywords
CFD, Adams, Friction, Friction coefficient, Turbocharger, Wastegate

WOLF, J.*Analýza koeficientu tření obtokového ventilu turbodmychadla.* Brno: Vysoké učení technické v Brně, Fakulta strojního inženýrství, 2019. 50 s. Vedoucí Ing. Petr Krejčí, Ph.D.

Prohlašuji, že jsem diplomovou práci na téma Analýza koeficientu tření obtokového ventilu turbodmychadla vypracoval samostatně s použitím odborné literatury a pramenů, uvedených na seznamu, který tvoří přílohu této práce.

24.5.2019 _____

Bc. Juraj Wolf

I would like to express my gratitude to my supervisor Ing. Petr Krejci, Ph.D. for willing approach and cooperation. Many thanks go to Ing. Jakub Planka and Ing. Adam Ondrejka for providing a flow bench which make the experimental part of this thesis possible. Special thank goes to my family supporting me over my studies.

Bc. Juraj Wolf

Content

1. Introduction

The automotive industry is under pressure due to the requirement from costumes and governments for enhancing the efficiency of combustion engines and its downsizing. One of the techniques used is supercharging.

Most common branch of supercharging are turbochargers. Turbocharger technology was developed in the early 1900s. At first of all, it found its usage in the aviation industry, and mostly during the second world has advanced rapidly. Numerous fighter and bomber planes were equipped with the turbocharger, which increased their power and efficiency. Turbochargers started to be a common part of personal vehicles only since the 1980s. Late implementation to the automotive industry was caused by their reliability issues [1]. Since than Turbocharger technology has come a long way and nowadays can be considered as well managed technology. Although, like in case of any technology are still improvements that can be made.

The focus of this diploma thesis aims at the investigation of friction in bypass valve used for regulation of turbocharger. More specifically friction between the valve and its bushing. As it is seen in figure 1.1, this system is very complex in terms of geometry to evaluate friction conventionally. The new method needs to be presented. This diploma thesis was made in cooperation with Garrett advance motion company

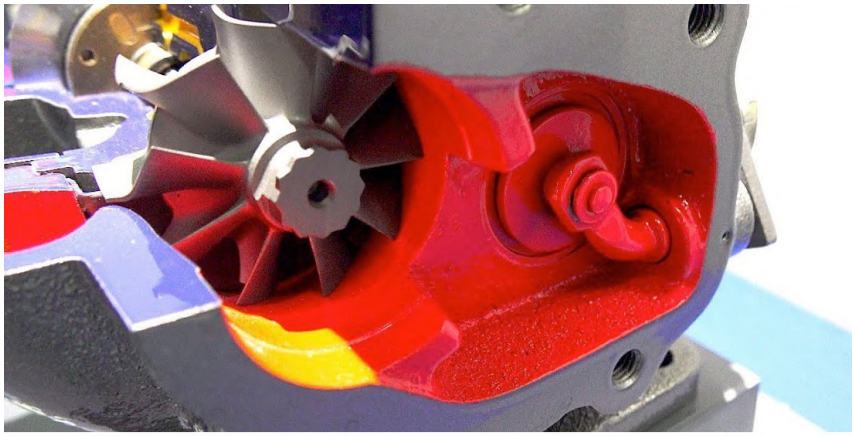

Figure 1.1: Wastegate system in turbocharger [2]

.

2. Brief overview and goal definition

Waste-gate system works under very extreme conditions such as thermal cycling, pulsation loading, high temperature, etc. For a proper and long-life design, it is crucial to have deep knowledge of each element of the system. One of the concern is a friction coefficient between the shaft of the valve and bushing. Friction has an impact on two very important aspects. Where one of them is life-cycle and the other is actuator matching which is the process of selecting actuator for a given application. The main purpose of this thesis is to create a method that would allow evaluation of the friction coefficient in the bypass valve system. Work diagram of the thesis shown in the figure 5.8. Key points of the thesis are as follows:

- Create a design of the test fixture for the experiment.
- Conduct a CFD simulation to evaluate aerodynamic force acting upon the valve in the test fixture.
- Create a model of the kinematic chain of the fixture.
- Compare results from simulation and experiment.
- Evaluate the friction coefficient for given parameters of the bushing and valve.

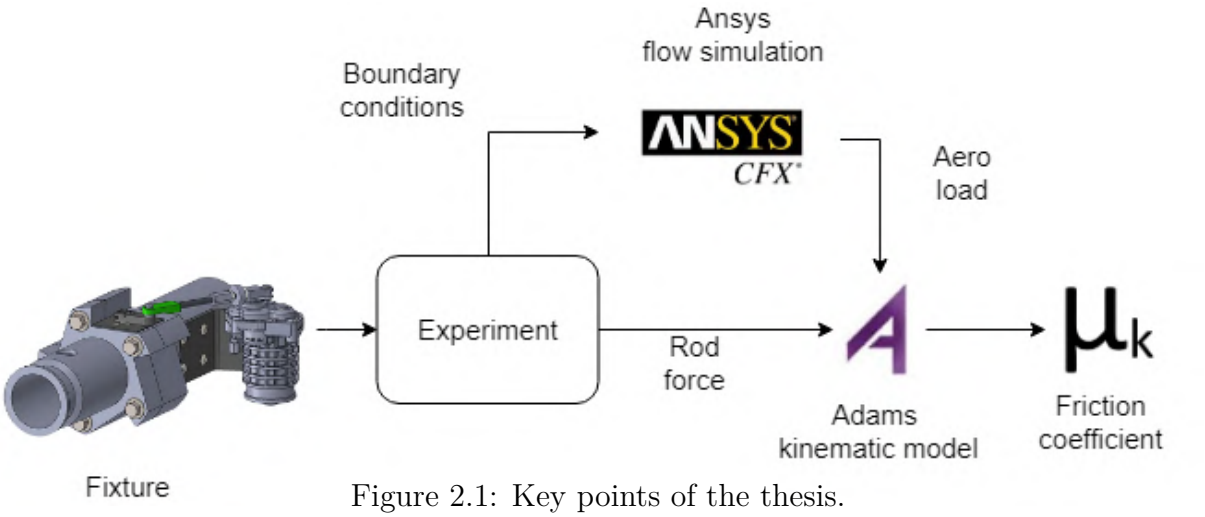

Figure 2.1: Key points of the thesis.

3. Turbocharger

A turbocharger is a rotary machine that is mostly used in the automotive industry. The function of the turbocharger is to raise the amount of air delivered in engine cylinders. Usually, this amount is limited by atmospheric pressure. This limitation affects the engine power output, which depends on the air/fuel ratio. By compression, more air is pumped into the cylinders which arrive as power increase. By utilizing exhaust gas energy, turbocharger increases the overall efficiency of a combustion engine [3].

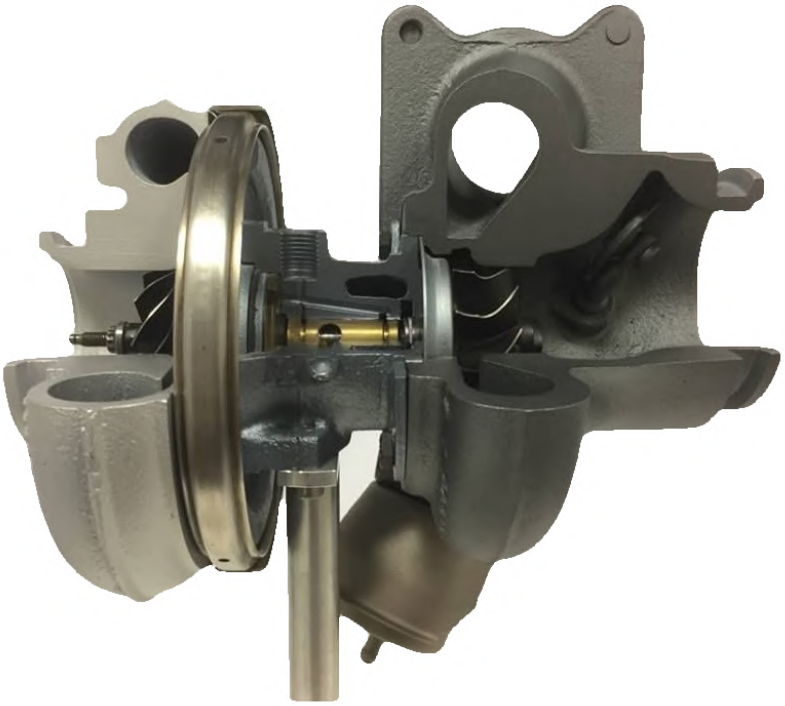

Figure 3.1: Cross-section of the Garrett turbocharger model.

Even though an increase in power and efficiency are certain advantages; the turbocharger has its issues. First of all, the turbocharged engine requires a lower compression ratio than non-turbocharger engines. Lower compression ratio causes that engine runs less effective at low power output. Another issue that turbochargers suffer from is effect called turbo lag. Because turbocharger uses power from exhaust gases, the turbine wheel needs a build-up in the form of exhaust energy to power a compressor wheel. Due to the inertia of compressor, turbine wheel and shaft that connects them, the turbocharger is unable to provide the high boost instantaneously when the engine is speeding up. In other words, the driver needs to speed up before turbocharger starts to operate. Based on the size of turbocharger, the lag can last up to seconds before noticeable boost is delivered. Another drawback relates to mass flow over the compressor. Two critical situations can occur, surge, and choke. Surge happens when the mass flow over the compressor is rapidly reduced by increased pressure ratio between inlet and outlet of the turbocharger. Surge is then an operation point where the flow of air reverses and the compressor wheel becomes unstable. Surge can severely damage or even destroy the compressor wheel. Needed to say that compressor does not stop or start to spin in another direction, only the flow

of the gas reverses. The other extreme, choke, occurs when mass flow increases rapidly through the compressor. This effect happens when the sonic condition is met in a certain place in the turbocharger. After this point, no mass flow can be passed through. Both of these extreme are crucial for the design of turbocharger. Each engine in the process of design has a specific so-called compressor map, shown in figure 3.2, that takes these extremes in consideration [4], [5].

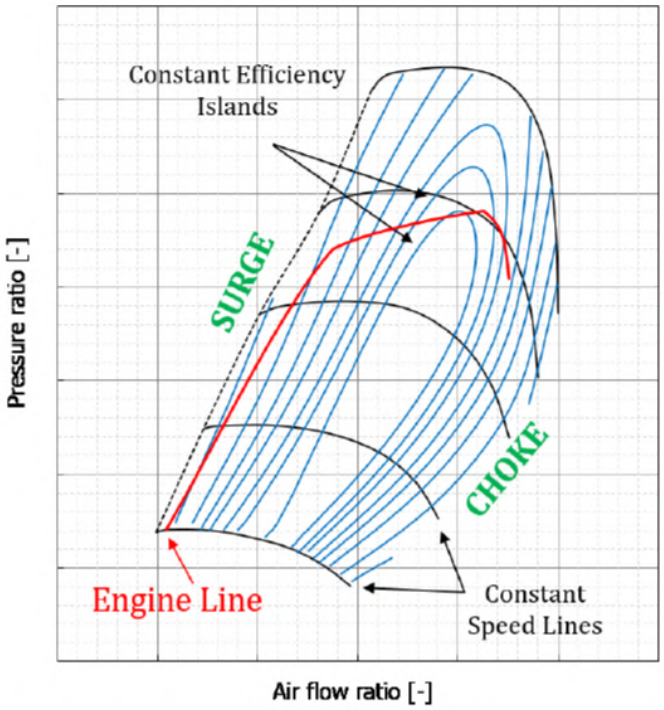

Figure 3.2: Compressor map of turbocharger [4].

3.1. The principle of turbocharger operation

A work-flow of the turbocharger is shown in figure 3.3 At the begging of the process, air goes through filters and continues on compression wheel(point A). Behind the compression wheel, we obtain air with higher temperature, pressure, and density(point B). After compression, the air is supplied to the inter-cooler where the air is cooled down, which results as a density increase. By increasing the density in inter-cooler, volumetric efficiency rises, and the risk of detonation burning decreases. Afterward, the air is fed to the engine, mixed with fuel and burned. Exhaust gas continues through a volute (point C) to turbine wheel which is placed on a common shaft with a compression wheel. Gas is then dumped into the atmosphere (point D) [6], [7].

3.2. Construction of the turbocharger

The turbocharger can be divided into 4 main parts which are compression, central, turbine part and control system.

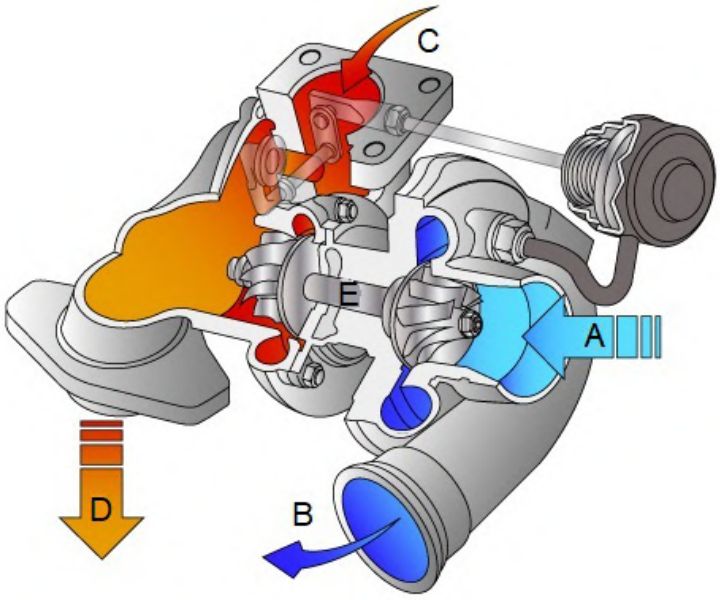

Figure 3.3: Working principle of the turbocharger [8].

3.2.1. Compressor

The mentioned section consists of three crucial components such as compression housing, wheel, and diffuser shown in figure 3.4. Beside these component's, compression housing may contain pressure sensor and bracket for the actuator of the control system[6].

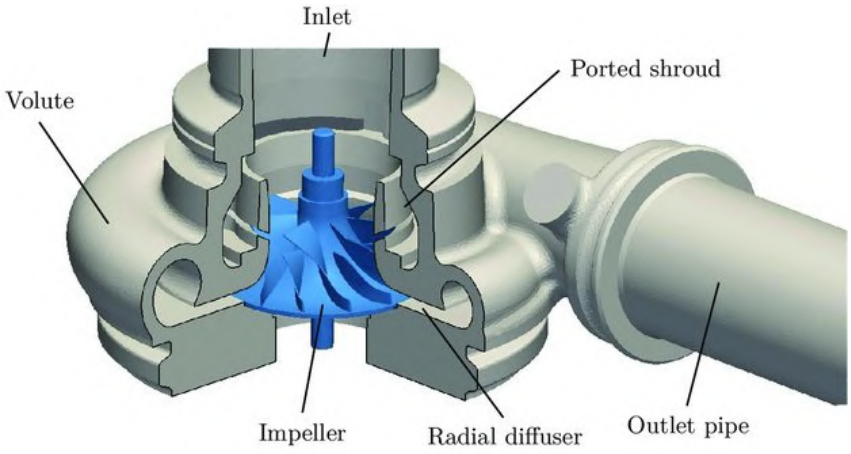

Figure 3.4: Compressor housing [9].

The advantage of centrifugal compressors is that they can pass an enormous amount of air relative to their size. By high-speed rotation of the wheel, the air is drawn in the axial direction, accelerated and expelled in a radial direction. Purpose of the diffuser is to slow down high-velocity air causing pressure and temperature increase. In the volume of the compressor, housing is air collected and slowed down further. In compression housing, the air is pressured by the kinematic energy of the compression wheel. Compressor housing

is exposed to high vibration and temperature around 180°C. The most common material for turbocharger compressor are aluminum alloys[6].

3.2.2. Central section

The primary function of a central assembly is to bear a common shaft of the compressor wheel and turbine wheel. Simultaneously it provides an oil supply and cooling for the rotary system. Axial and radial bearings hold the shaft and allow it to rotate. The bearing system is designed in a way that there is no contact between shaft and bearings which are provided by the thin oil film. Besides, oil film has a damping function, which contributes to the stability of the rotor[6]. In the cross-section of central housing shown in figure 3.5 can be seen an oil distribution to bearings. Vast majority turbochargers utilize the thrust bearing. However, part of the development focuses on replacing the thrust bearing system with ball bearing and use water as a cooling medium. The main advantage of this replacement is that ball bearing increase the durability of the system and transmits power more efficiently to the compressor wheel. Few arguments speak for using water as a cooling medium. Firstly it is more reliable than oil. Secondly, it helps stabilize temperatures and prevents the oil from choking in housing [5]. The whole system can achieve speed up to 130,000 RPM. Also, the shaft must resist extreme pressures and an enormous thermal gradient where on compressor side may be temperatures about $150°C$ and $1000°C$ on the turbine side [10],[11].

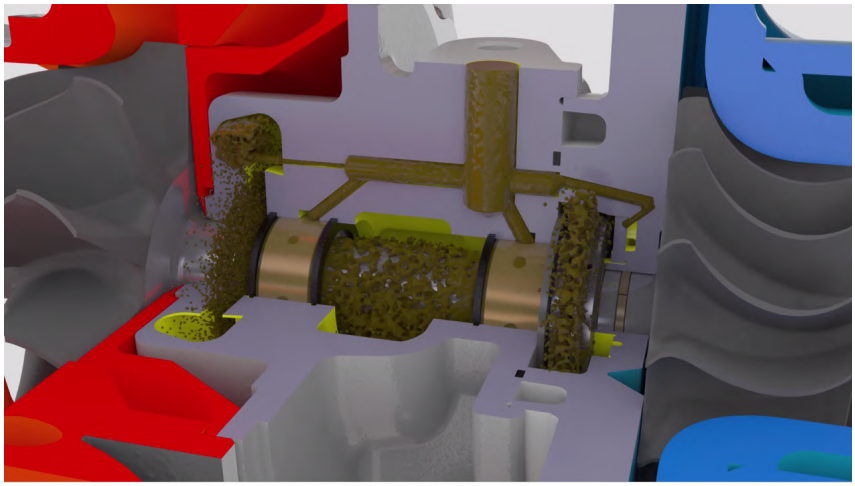

Figure 3.5: Cross section of central section[12].

3.2.3. Turbine section

Turbine section consists of a turbine wheel and housing. Role of the turbine assembly is to use the energy of the exhaust gas to drive the compressor wheel. This conversion to mechanical energy appears as a temperature and pressure drop between inlet and outlet. Exhaust gas is accelerated in volute and directed to the circumference of the turbine wheel at a proper angle. The turbine wheel is designed to convert almost all the kinematic energy into shaft power.

Turbines can be divided by the direction of the gas flow applied on the turbine wheel into radial and axial. The radial turbine wheel is mostly used in automotive whereas axial are used for application with a higher power output [6]. Furthermore, volute, base on design, can be divided either as a single or multi-entry. Single entry volute is a more straightforward solution and more appealing to manufactures for its cost. However, engine cylinders create an unsteady flow. This pulsation from engine tends to overlap, and multi-entry scroll offers a solution. The manifold is split by a screen creating two tracks leading onto turbine wheel. Each section is adjusted, so pluses come on a turbine wheel out of phase [5].

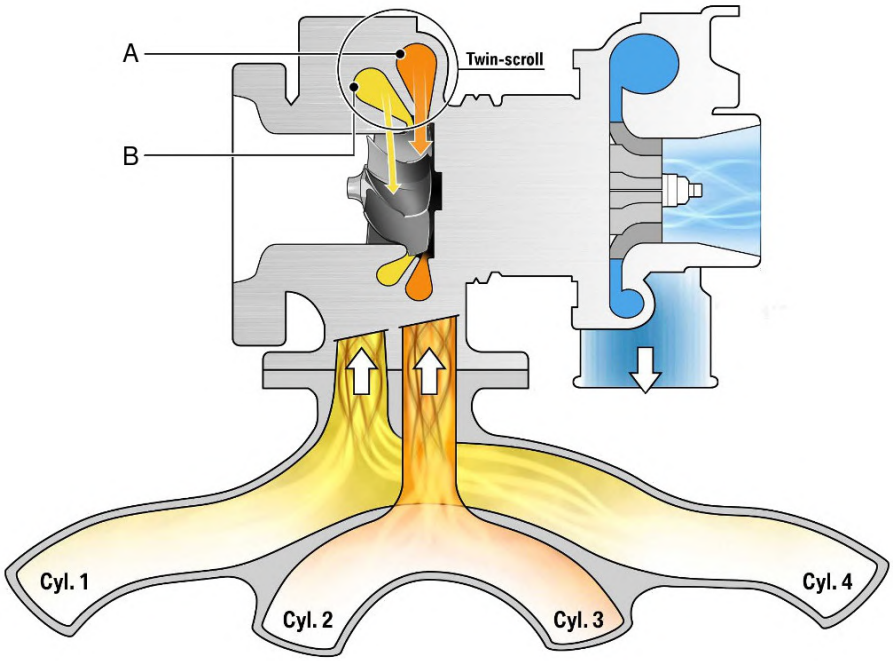

Figure 3.6: the work principle of twin-scroll [7]

In figure 3.6 can be seen such volute with two spiral-shaped channels. Each of the channels of the twin scroll has its function. Channel A collects exhausted gases from cylinders 2 and 3 and directs them on the outer edge of the turbine wheel. This channel results as an enhancement in terms of rotation speed. Smaller channel B, which collect exhaust gases from cylinders 1 and 4, streams exhaust gas on the inner part of the turbine wheel. This set up improves the dynamics of the turbocharger by reducing already mention turbo lag. This design is mostly used for heavier vehicle and combines power increase and the better response of the turbocharger [7].

3.3. Control system

One of the turbocharger requirements is to provide same power output at all engine speeds from operation range. To obtain high power out at the low speed of the engine may cause difficulties because exhaust gas has not got enough energy to drive the turbine wheel to provide the desired boost. On the other hand, at very high engine speed, turbine wheel may be accelerated to high speed and cause over-charging of the engine. By increasing

the boost pressure over allowed limits, the risk of knocking rises as well. To secure the optimal boost pressure, a control system takes place. The regulator controls the amount of exhaust gas applied to the turbine wheel. The most common methods are [3]:

- Waste-gate
- Variable nozzle turbine (VNT)
- Two stage turbocharging

3.3.1. Waste-gate

Waste-gate is the simplest kind of regulation of turbocharger. It is mostly used for a gasoline engine with low power output. Waste-gate system composes of a valve controlled by the actuator and a blow-off channel. In case of high boost requirement, the channel stays closed. At a certain point when the boost is reached valve opens, and exhaust gas goes through the channel instead of the turbine wheel. By opening the channel pressure difference between inlet and outlet of the turbine decreases, therefore, the turbine slows down. Based on constructional arrangement waste-gate we can categorize waste-gate into two groups, internal and external[3].

Figure 3.7: Internal waste-gate [13].

Internal Waste-gate is directly built in the turbine housing(figure 3.7). Channel, which is closed by the valve, is situated before the turbine wheel. The valve is welded to a crank and linked to the actuator by rod and actuator crank. Bushing, which is embedded in housing, bears the valve and support its rotation. Depending on the relative position of the linkage, we can distinguish a lever mechanism in the shape of letter U or Z. On the end of the kinematic chain is an actuator which is fixed to a bracket and usually placed on the compressor housing. Movement is provided by a hydraulic, pneumatic, or electric actuator.

Furthermore, the actuator can be categorized based on motion to linear or rotary. In the automotive industry, pneumatic actuators are the most favorite for their simplicity and low price. Although electrical actuators are implemented more often due to better controllability of the wastegate valve compared to pneumatic actuators. Hydraulic is mostly used for larger application such as boats or small plains [3],[7].

Figure 3.8: External wastegate [14]

An external wastegate, shown in figure 3.8,is connected to a pipeline between compressor and engine on one end and turbine volute on the other. In case of over boost, high pressure on the compressor side opens the channel and dumps the air into the atmosphere. Advantage of the external over the internal is packing and the fact that there is no need for an actuator. Also, dumping air to the atmosphere prevents the turbulent flow which causes back-pressure on the turbine which lowers the overall efficiency and may cause damage to the turbocharger [7], [15].

3.3.2. Variable nozzle turbine

VNT (Variable nozzle turbine) regulates the flow of the exhaust gas on the turbine by changing the throat area between its vanes as shown in figure . VNT mechanism consists of rotary vanes placed in cartridge. Vanes are connected to unison ring via arms. By rotating the unison ring vanes rotate simultaneously. Unison is connected via the main arm to very same kinematic chain as in case of waste-gate.[7].

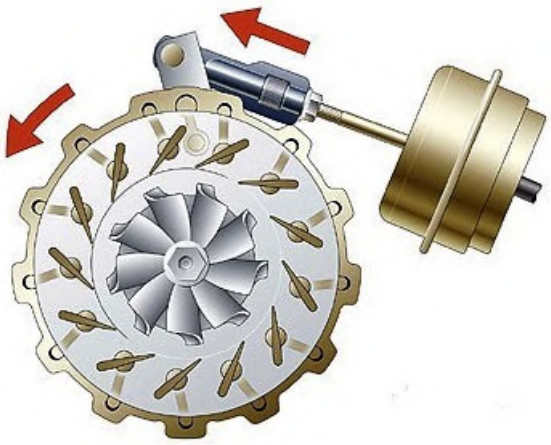

Figure 3.9: VNT regulation [7]

Rotation of vanes adjusts the gas flow through the cross-sectional area between vanes. At low engine speed, the active area is reduced by closing the vanes. Exhausted gases are then directed onto the turbine wheel under a smaller angle; therefore, conversion of exhaust gas energy to mechanical is more effective. Also, the pressure ratio across the turbine increases; thus, the velocity of exhaust gas rises and produce more boost. Vanes are opened at high engine speed. This results as a speed drop and exhausted gases flow on turbine wheel in angle nearing to 180° which is less effective [3].

VNT provides considerable higher torque at low speed. Compared to waste-gate, torque can improve by 40 % . Also, engine torque response is faster. On the other hand, VNT has a lot of moving parts, therefore, the risk of damage increases [3].

This type of regulation is more suitable for medium and heavy duty cycle vehicles [7].

3.3.3. Two stage turbocharging

Two turbochargers realize this method. Turbochargers can be in either parallel or serial connection. One of the turbocharging is smaller than the other. The smaller turbocharger has smaller inertia and therefore takes over the function at low engine speeds. On the other hand, larger turbocharger takes over from higher engine speeds. This arrangement improves transient performance and low-speed torque. A bypass valve regulates the stream of exhausted gases. In the closed position, all gases go on turbine wheel of smaller turbocharger. If the valve opens, gases flow on the turbine wheel of a larger turbocharger.

This assembly work base on engine speed in three regimes:

Bellow 1500 RPM, This operating range is shown in figure 3.10 on the top scheme. Only the smaller turbocharger fulfill the compression function. The bypass valve is closed, and all exhaust gasses are directed on turbine wheel of smaller turbocharger. After gases pass the turbine wheel of the smaller turbocharger, they flow on the turbine wheel of lager turbocharger but with significantly less energy.

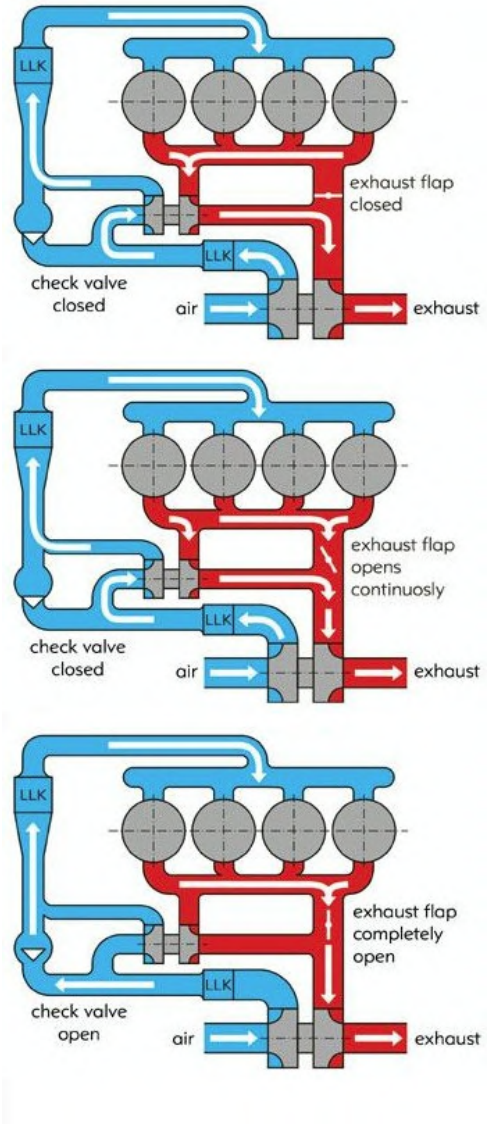

Figure 3.10: Two stage turbocharger [16].

From 1500 RPM to 2800 RPM in this operating point, shown in the middle scheme in figure 3.10, a bypass valve opens and gases flow directly on both turbine wheels. Valve opening angle is regulated based on the mode of driving and the required boost. At compressor side, the compressor wheel increases the pressure by 2 to 2.5 times. In the second stage is this pressure increased another 2 to 2.5 times.

Above 2800 RPM at this point valve at the turbine side is fully opened and gases in manifold go only on the turbine wheel of second stage turbocharger. At compressor side, the smaller compressor is weaned from the circuit, and compressed air is flowing only through second stage turbocharger straight to the engine. This stage corresponds to schene on the bottom of the figure 3.10

This method also increases the durability of the bearing due to smaller pressure differences between inlet and outlet on both compressors wheel [16].

.

4. Friction

Friction plays an important role in the control system of the turbocharger. There are friction forces in every joint of the lever system. In the case of wastegate, the most significant source of the friction force is contact between the shaft of the valve and bushing that holds the shaft. As is described in the chapter 4.5, friction has a significant impact on actuating force.

In general, friction occurs between two surfaces in contact and appears as a mechanical force which resists their relative motion. It is a form dissipation of the energy usually as heat or deformation. Friction forces can be defined by the given equation [17]:

$$F_f = \mu F_n \tag{4.1}$$

Where μ is a friction coefficient and F_N is the normal force that presses surfaces together. The friction coefficient is unique for a given system and involves factors such as as[18]:

- Roughness of the surface
- Relative velocity
- Type of movement
- Environment
- Type of material of the mating surfaces
- Presence of lubricating film
- Contamination

Even though there are tables with a friction coefficient for specific mating materials, textures, lubricants and more. However, it is quite straightforward that the coefficient of friction is an extremely complex description of a system. Thus using values of the friction coefficient from tables is a gross estimation. To evaluate the friction coefficient as accurate as possible, it needs to be measured in a system. Impact of all factor mention above are well documented by Budinski in Guide to Friction, Wear, and Erosion Testing where the author also describes bullet points of standard ASMT G 115 on conducting any friction test and recording test data [18].

Friction can be distinguished as external or internal. External friction or resists movement (kinetic) between sliding or rolling surfaces. Friction coefficient differs by type of movement. The highest coefficient of friction is always static when there is no relative motion between surfaces. The friction force is then the reaction to resultant of all tangential forces acting upon a body. After applied force overcomes the static friction force and the surface starts to slip, static friction is subsidies by dynamic friction. The dynamic friction coefficient is always less than the static [17].

As internal friction can be classified as friction between lubricant molecules which is described as viscosity [17],[19].

There are several models of friction. Some of them are presented in the following chapters. Given models are based on Coulombe fiction model. There have been several studies that have compared different types an included more complex and accurate model

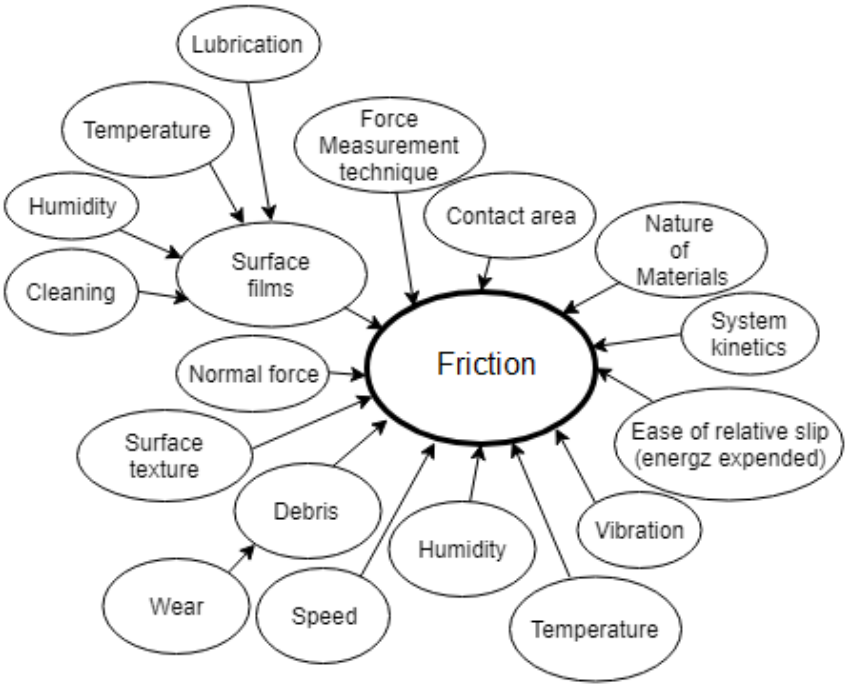

Figure 4.1: factors affecting friction force [18].

such as Dahl, LuGre, Gonthier, etc. For example, a study of T. Tjahjowidodo et al. where authors compare different types of friction model and use them as a feedforward controller for a DC motor. Conclusion of their study was that even though coulomb based models do not provide accurate results at low velocities, they can provide comparable results to the advanced models at high velocities[20]. Great overview of mention models and more provide a study of Ettore Pennestri et. al. The study presents 8 different models and focuses on the trade-off between performance in terms of computation power, numbers of parameters required and capabilities to represent phenomena such as Stribeck effect, stiction, and pre-sliding displacement. [21].

4.1. Coulomb model

Coulomb model is one the simplest model of the friction and represent friction on the macroscopic level very well. This model describes the discontinuity between friction force and velocity. The following equation expresses friction force [22]:

$$F_f \begin{cases} \leq \mu_s F_n & \text{if } v = 0 \\ = -\mu_k F_n sign(v) & \text{if } v \neq 0 \end{cases} \tag{4.2}$$

Where F_f is friction force, F_N normal load acting upon a body, μ_s and μ_k are static and kinematic friction and v is relative velocity.

As seen in figure 4.2 and described by equation 4.2 if $v = 0$ therefore no slipping occurs friction force is equal to resultant of tangential forces and takes up any value from 0 to F_s. If $v \leq 0$ friction force remain constant either $-F_d$ or F_d.

There are two major issues with Coulombs model, discontinuity and the fact that experiments show that friction also depends on the value of the relative velocity[22],[21] .

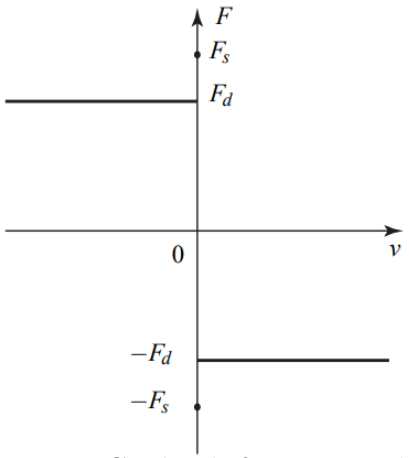

Figure 4.2: Coulomb friction model [21].

4.2. Smooth Coulomb model

Smooth Coulomb model overcomes the discontinuity of the previously described Coulomb model. As seen in figure 4.3, at velocities approaching zero, the discontinuity is replaced by smoothening function. Several functions can be used such as linear, trigonometric or exponential. An example of such a function is hyperbolic tangent [21]:

$$F_f = -F_n \tanh\left(\frac{v}{v_d}\right) \tag{4.3}$$

Where v_d is a velocity tolerance. Given model is more computational stable due to the elimination of the discontinuity. However, it is not possible to simulate static friction by given model since at $v = 0$ is the force equal to null [21].

4.3. Velocity based model

Velocity based model is built on the idea of the previous model but unlike smooth Coulomb model, this involves static friction. Although, as seen on figure 4.4 this model still cannot represent friction behavior at zero velocity. Parameters required for the model are v_s, v_d which represent velocity tolerances or thresholds for a static and dynamic friction coefficients respectively and μ_s, μ_d which are friction static and dynamic friction coefficients. Given model is implemented in commercial software MSC Adams [23], [21].

Wang and Rui present in their paper similar model by the following equation. The given friction coefficient is a function of relative velocity v [24]:

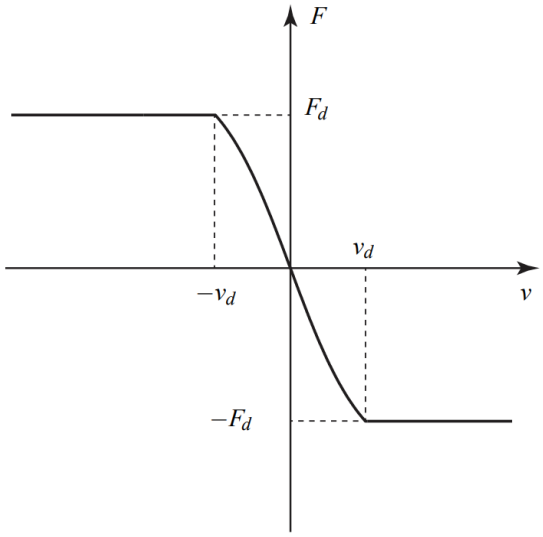

Figure 4.3: Smooth Coulomb model [21].

$$\mu = \mu_s \sin(C \arctan(B v) - E(B v - \arctan(B v))), \tag{4.4}$$

where μ_s is the static friction coefficient and coefficients B, C, and E are varied until the curve matches the experimental force. Figure 4.4 shows force behaviour based on equation 4.4

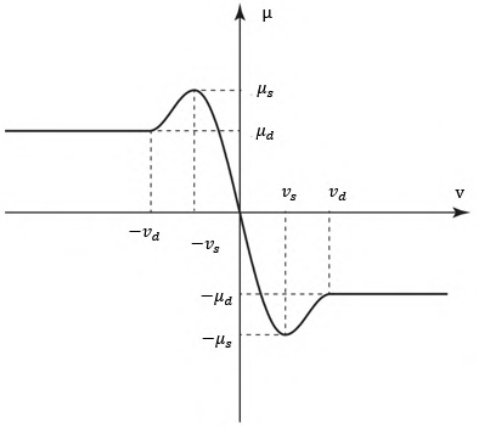

Figure 4.4: Velocity based model [21].

4.4. Coulomb model with a viscous friction

As mention earlier in this chapter, the friction force is also dependent on relative velocity. Following equation express the behavior of viscous friction [22]:

$$F_f = k_v v \tag{4.5}$$

Where k_v is a viscous friction coefficient and v is a relative sliding. In other words, the friction force is proportional to the velocity. This describes friction between two lubricated contact surfaces but does not represent the behavior of dry contact friction.

By adding a viscous factor to Coulomb friction model we may get a more accurate and representative model described by following equation [22]:

$$F_f \begin{cases} \leq \mu_s F_n & \text{if } v = 0 \\ = -\mu_k F_n sign(v) + k_v v & \text{if } v \neq 0 \end{cases} \tag{4.6}$$

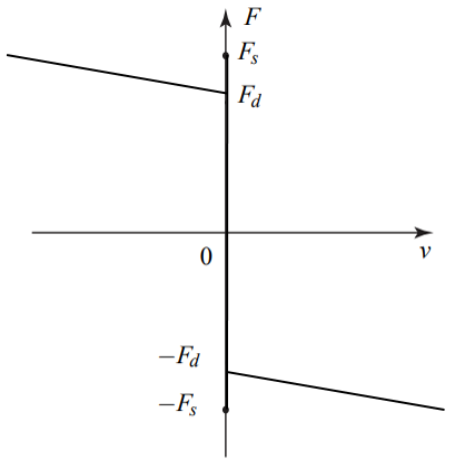

Figure 4.5: Viscous friction implemented in Coulomb model [22]

This model still suffers from a discontinuity at velocity $v = 0$. But this can be easily overcome by an implementing smoothing function and velocity thresholds as mention in previous chapters.

4.5. Friction in waste-gate system

Kinematic chain of the turbocharger is a four-bar mechanism. Output (valve side) and input (actuator side) links are in this terminology called cranks. Cranks are connected via a coupler (rod). Friction occurs in the wastegate's kinematic chain in each joint and between a bushing and a valve. The friction force between the bushing and a valve is more significant than friction forces in joints combine.

Direct Measurement of the friction force between the valve and its bushing is very problematic due to their geometry. It is more convenient to measure the friction force indirectly on the kinematic chain. From a practical point of view, the simplest solution is to put a load cell on the rod of the kinematic chain

With no presence of friction, force record from load cell placed on rod would be the same curve disregard the valve opening or closing. On the other hand, Presence of friction extend the curve and creates a hysteresis loop. The bigger the friction, the wider the loop.

Based on static equilibrium shown in figure 4.6, the following equations can be expressed:

$$M_{rod} + M_f - M_{aero} = 0 \qquad M_{rod} - M_f - M_{aero} = 0 \tag{4.7}$$

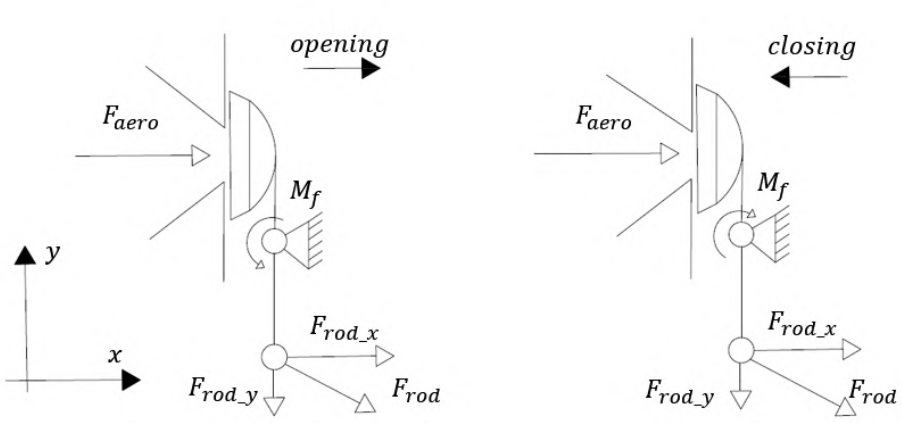

Figure 4.6: Kinematic layout

Where M_{rod} is torque caused by force acting in rod and provided by the actuator,M_{aero} is torque caused by aerodynamic load F_{aero} and M_f is torque caused by friction force. Figure 4.7 shows a rod force behavior during the opening and closing, based on equilibrium and assumption that the valve opens a closes at constant angular velocity. When the valve opens, the torque caused by friction forces opposes the torque caused by the aerodynamic load. In this case, friction torque helps the actuator. Nonetheless, when the valve closes, the actuator has to overcome torque caused by the aerodynamic load and the friction torque. Friction forces in the valve/bushing system arise at pads of the valve where they come in contact with bushing. Normal forces that act upon such pads depends on rod force, aerodynamic load, and the geometry of the valve.

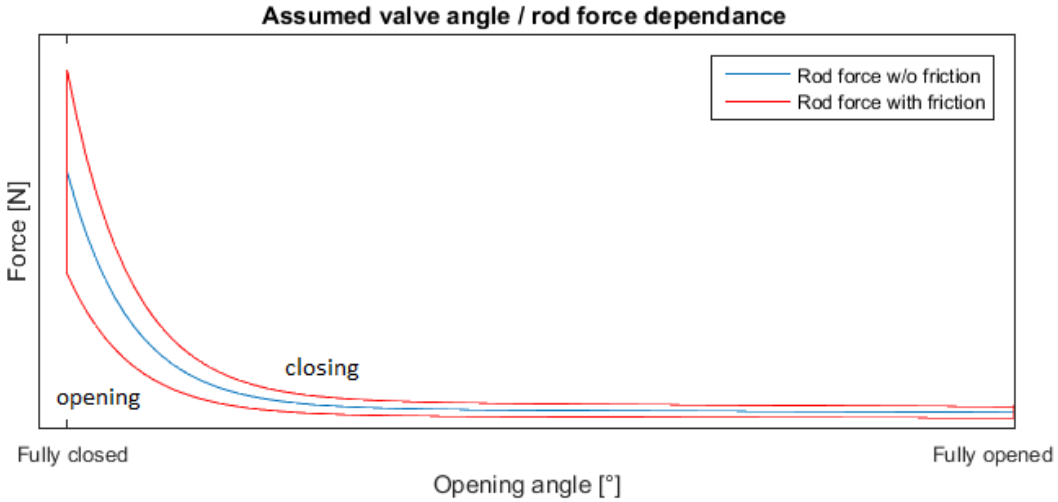

Figure 4.7: Assumed rod force behavior.

.

5. Experimental set up

The idea of this thesis was to design an experiment, that would allow evaluating a friction coefficient between the bypass valve of the turbocharger and bushing that supports it. There were several demands regarding the design:

- The design of the kinematic chain should be similar to the one used at the turbocharger.
- The design of the test bench should allow testing of various types of valve.
- Acting force upon valve should be aerodynamic.
- Result from an experiment must be validated by simulation tools.

Figure 5.1: Valve and bushing.

5.1. Fixture design

One of the most crucial key points of this thesis was to create a test fixture. The fixture was designed in commercial software Solidworks. The whole assembly with all its features is shown in figure 5.3. Figure 5.2 shows detailed description with nomenclature.

Each side ends with a V-bend connector, which enables it to be connected to pressure source on the inlet and acoustic noise filter on the outlet. On each side has drilled a hole for pressure sensors. Both sensors are placed as close to the valve as possible due to the accuracy of the CFD simulation.

There are 5 slots cut out on the circumference of the middle part. This feature allows testing more types of valve/bushing designs on the same fixture. Geometries of the valve may differ in the diameter of the valve and the distance between the center of the poppet

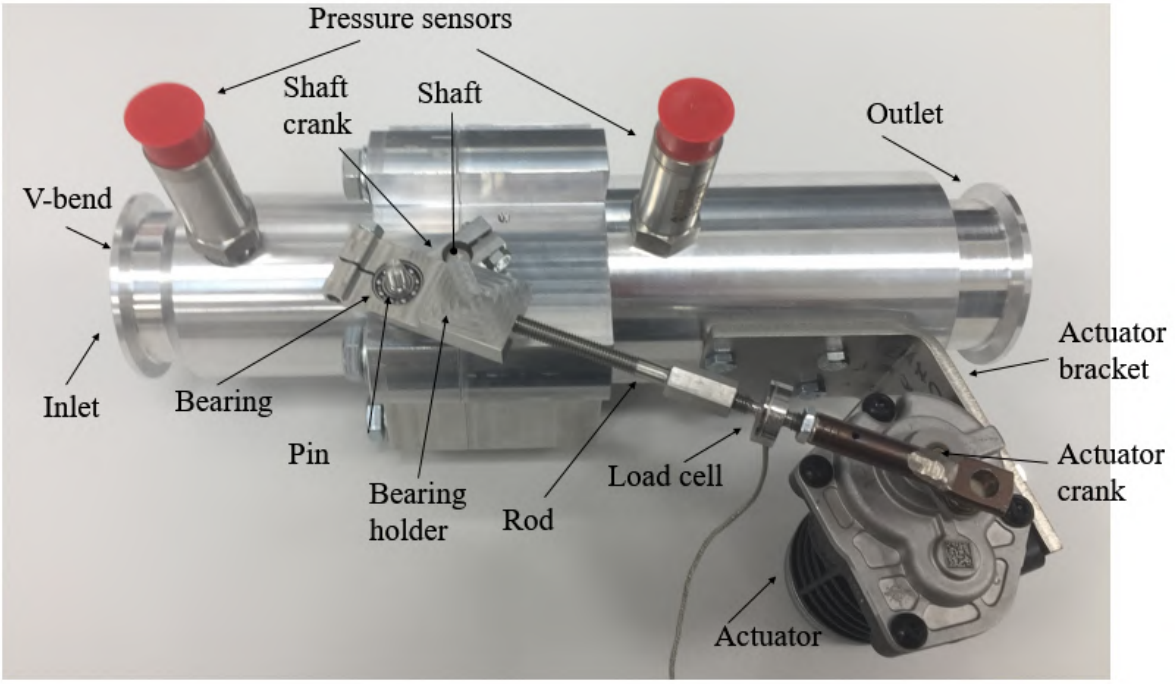

Figure 5.2: Fixture assembly.

and shaft. A conic saddle on the inlet of the fixture directs the gas on the poppet. The saddle is replaceable, so the inlet diameter of the channel could fit the design of poppet. The whole tube was manufactured from one piece and then cut in half, so valve and bushing are replaceable. The cut goes through the center of the hole for the bushing. There is a transitional fit between the bushing and the fixture. This fit ensures that bushing stays still, but the fixture does not deform the bushing. The cut of the fixture cannot violate the transitional fitting of the bushing hole. Therefore, the cut is performed as first, and then the hole is drilled. As the material for a body of the fixture was selected aluminum for its cost and lightweight.

The kinematic chain was designed similarly as in case of the turbocharger. The valve is attached to the shaft crank. Usually, only a pin connects the external crank to the rod. However, the pin connection is a source of dry friction. This friction would bring an unwanted expansion of the hysteresis loop of the rod force. Accordingly, initial contact was replaced with a ball bearing. Rod is practically a shaft with a thread which can be screwed into the bearing holder, so the length is adjustable. Load cell , for rod force measurement, is mounted on the rod .

Prior to the actuator selection, a draft of the kinematics has been made. The focus was aimed at three things:

- What torque must Actuator provide.
- Required position of actuator hard stops.
- Dependence between valve opening angle and actuator angle.

The design was made simultaneously in Solidwork and MSC Adams. The highest torque that actuator needs to counter is at the closed position. The requirement of the

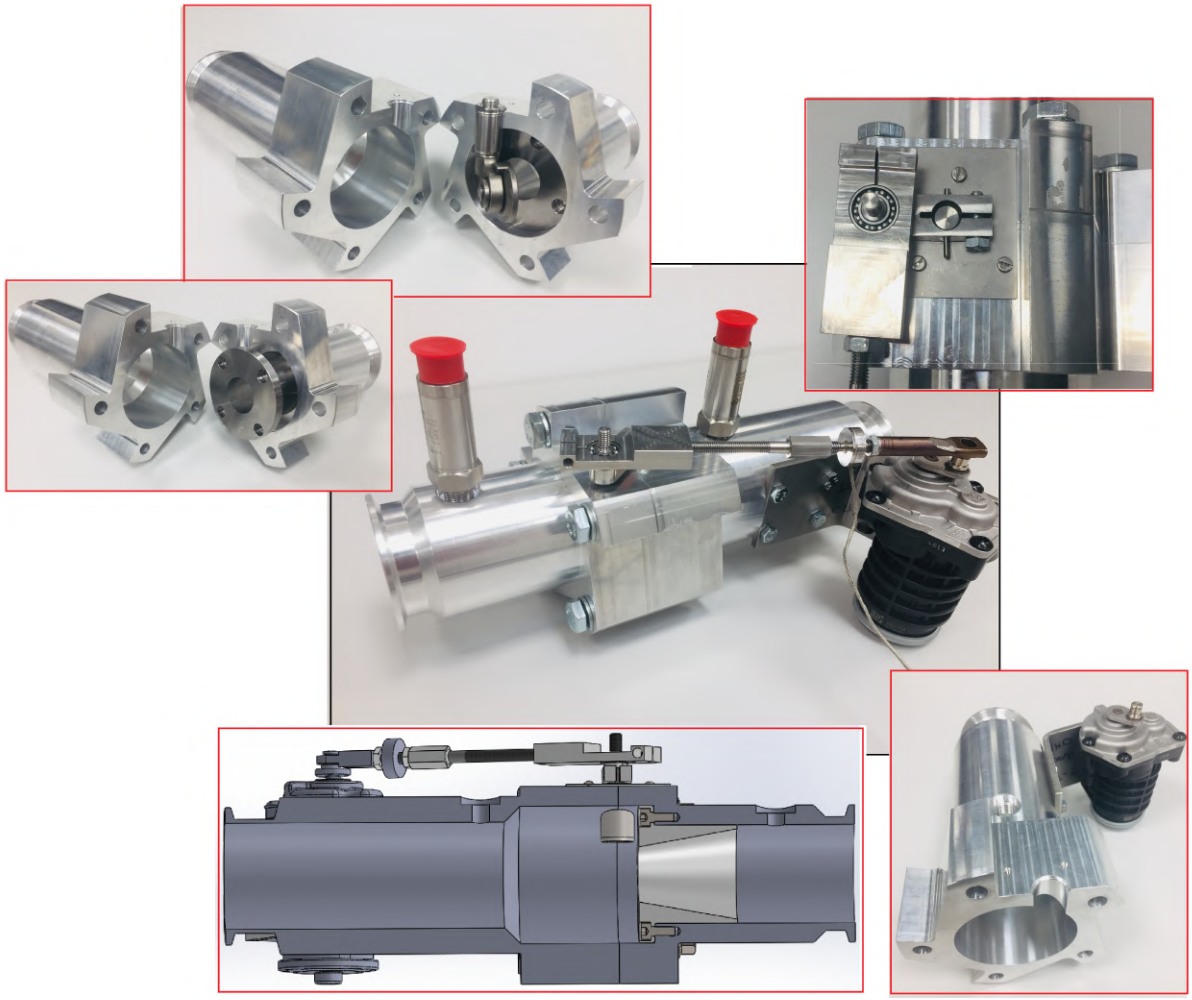

Figure 5.3: Fixture assembly.

pressure difference between inlet and outlet at the closed position was set approximately to 1.6 bar. In that case, the force acting upon the valve can be calculated by the following equation:

$$F_{aero} = \frac{p_{in}\pi d_c^2}{4} - p_{out}S_v \tag{5.1}$$

where,

- F_{aero} is a resultant force acting upon the valve.
- p_{in} pressure on inlet.
- p_{out} pressure on outlet.
- d_c diameter of the settle.
- S_v is surface of the back of the valve obtained from SolidWork.

After substitution, Force acting upon the valve is:

$$F_{aero} = \frac{270,000 \cdot \pi \cdot (28 \cdot 10^{-3})^2}{4} - 101,325 \cdot 1202 \cdot 10^{-6} = 44.46N$$

Once this force was evaluated, actuator torque could be calculated. Equations could be obtained from following sketch.

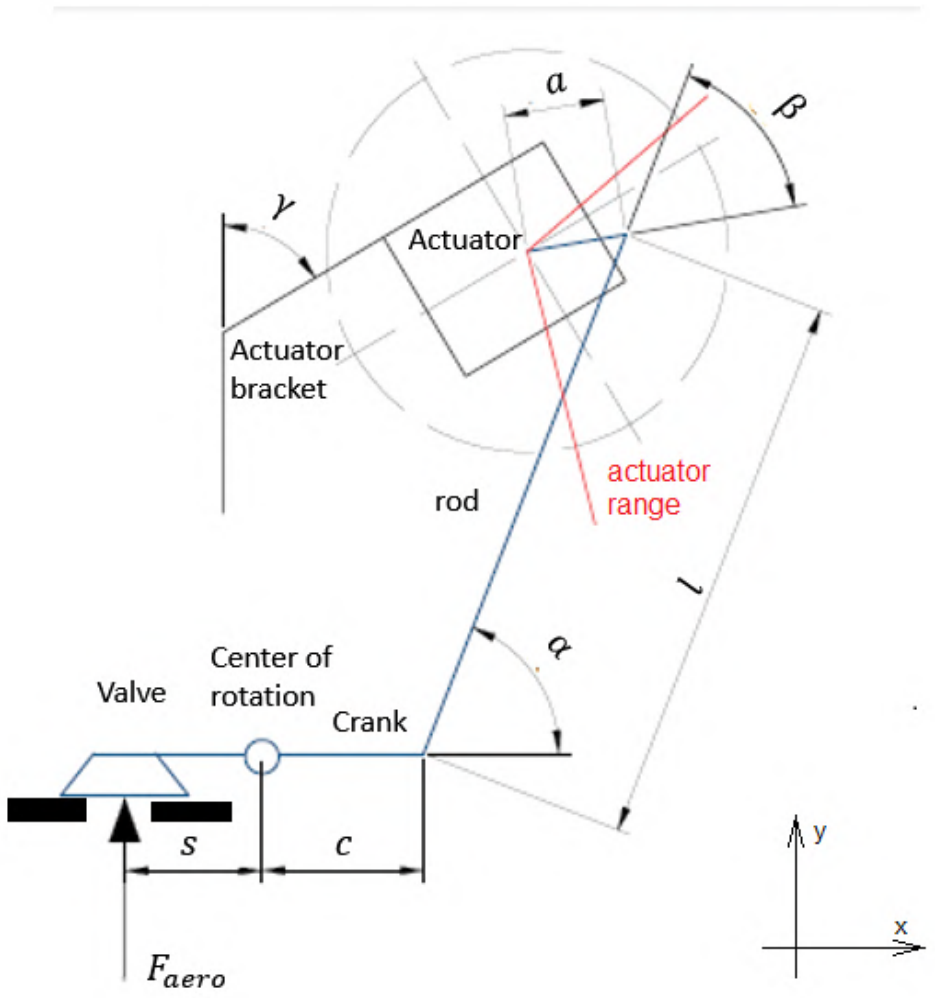

Figure 5.4: sketch of the kinematic chain.

From momentum equilibrium, force in rod can be expressed:

$$F_{aero} s = F_{rod} c \sin\alpha \tag{5.2}$$

$$F_{rod} = \frac{F_{aero} s}{c \sin\alpha} \tag{5.3}$$

consequently, needed torque provided by actuator:

$$M_{act} = F_{rod} a \sin\beta \tag{5.4}$$

$$M_{act} = \frac{F_{aero} s}{c \sin\alpha} a \sin\beta \tag{5.5}$$

$$M_{act} = \frac{44.46 \cdot 18}{23 \cdot \sin 68.28°} \cdot 13 \cdot \sin 61.54° = 428Nmm. \tag{5.6}$$

Development between valve and actuator angle needs to be considered as well.it is essential to know this dependence for control of the actuator to set the valve in the right position.. Since the kinematic chain is an asymmetrical four-bar mechanism, the aim was obtaining the dependence as linear as possible. This stage of design was conducted in Adams view. Figure 5.5 shows characteristic between actuator angle and valve angle of design four-bar mechanism.

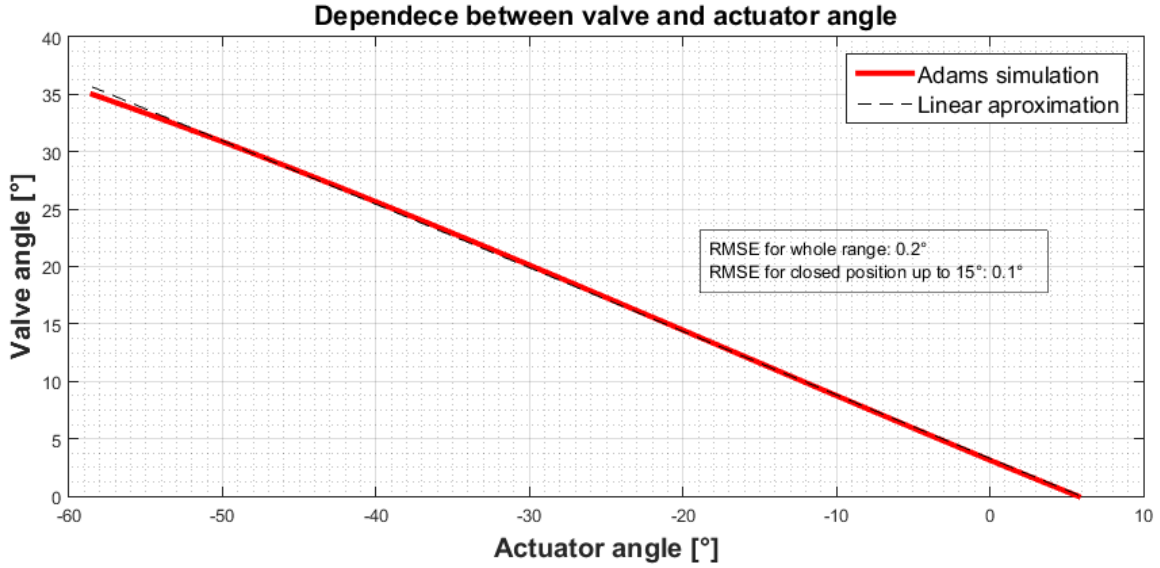

Figure 5.5: Dependence between actuator angle and valve angle.

A value that indicates the measure linearity between actuator angle and valve is a kinematic ratio between actuator crank and cranked connected to the shaft projected in axis x. The kinematic ratio r can be defined by the following expression:

$$r = \frac{c\cos\delta}{a\cos\theta} \tag{5.7}$$

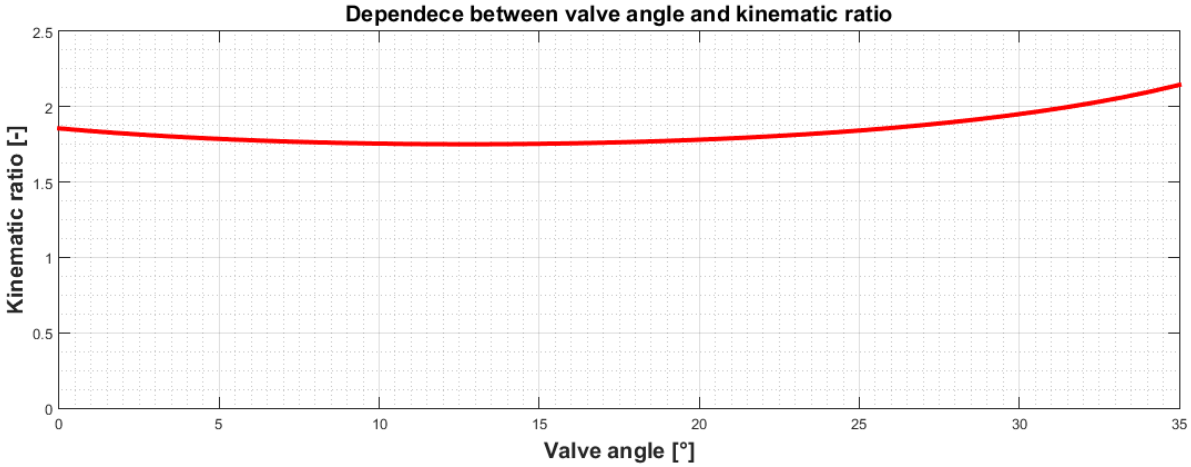

Figure 5.6: Development of kinematic ratio on valve angle.

where δ is an angle between crank of the valve and axis x, and θ is an angle between actuator crank and axis x. The more this ratio is constant more linear characteristic between actuator and valve angle we get. Kinematic ration can be modified by actuator position and by rod length. Angle between shaft crank and poppet of the valve has impact as well, but for more convenient construction was set to $180°$. Figure 5.6 shows development of kinematic ratio on valve angle .

Based on the design, geometry parameters and force requirements, actuator Kamtec L.generation 3 was selected. The motor of the of this actuator is PMDC brushed motor with nominal voltage 12V.This actuator has $110°$ range from hard stop to hard-stop. Maximum actuating torque is $600Ncm$ at ambient temperature $25°C$. The actuator has analog position feedback ranging from $0V$ to $5V$. As a control system was used hardware ultimate actuator drive box (UAD) made by the e-Tronics company. Via LabVIEW application was upload PID controller into the UAD.

Sensors PR-23YEi made by Keller company were chosen for pressure measurement. Range of these sensors is from 0 to 10 bars. This piezo-resistive pressure transmitter has a linear output voltage characteristic where $0V$ represent $0bar$ and $10V$ represent $10bars$. Pressure sensors measure relative to ambient pressure. Which in this case is atmospheric. For rod force measurement, loadcell LC201-500N by Omega was chosen. Load-cell is able to measure tension and compression up to 500N. The output from the loadcell was amplified in a load-cell/strain gauge amplifier SGA/A by Apllied Measurements LDT. company. Loadcell has a linear characteristic where 0V represents 0N and 10V 500N.

Mass flow was measured by senzor F-106CI by Bronkhorst company.

Setup of the all measurement devices is shown in figure

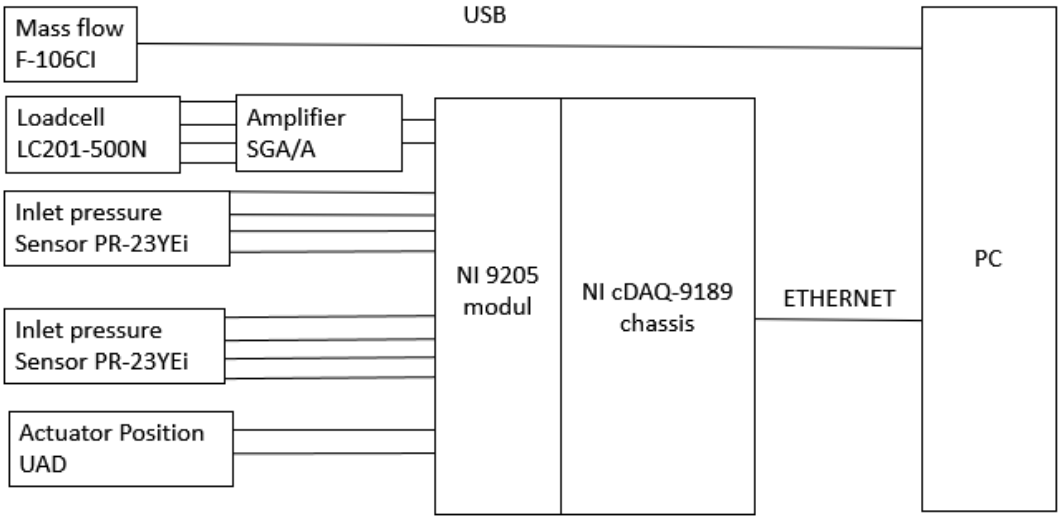

Figure 5.7: Setup up of the measurement.

.

5.2. Sample selection

To fit in bushing and valve into the fixture, small adjustments had to be done. Two parallel grooves were cut on the circumference. Grooves ensure that a small part of the bushing is aligned with the slot in the fixture. A bushing is then secured in position by a thin plate which is by screws pressed to the fixture.

A small hole was drilled in the head of the shaft perpendicular to the front face of the valve. The same hole is drilled through the shaft crank that is connected to the shaft. A small pin is then put through; this secures that crank and valve are fixed together and the angle between crank and poppet is 180°.

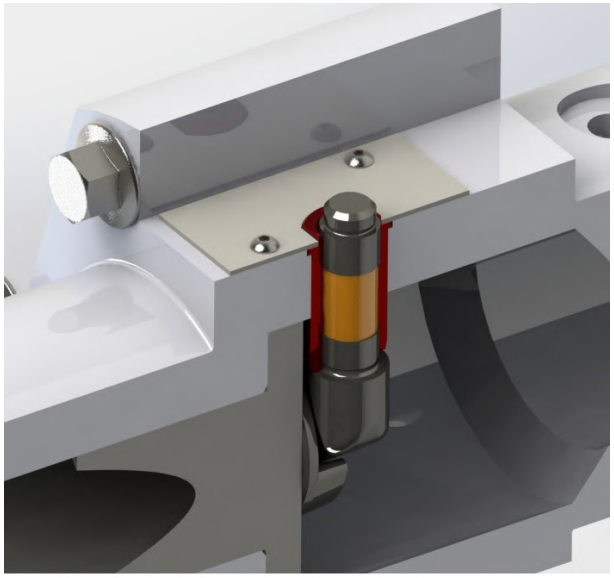

Figure 5.8: Fitting of bushing in fixture.

Factor such as roughness, material couple, and wear are tested to verify functionality of the fixture.

Roughness. Valve and bushing come into contact at valve pads. Therefore, the roughness of pads has an impact on the friction coefficient. Four samples with adjusted pads to roughness values Ra 0.2, Ra 0.4, Ra 0.6, and Ra 1.2 were selected. The assumption is that with increasing values of Ra, the coefficient of friction rises as well.

Material couple. The material of the shafts remain unchanged, and only material of the bushing is varied. Prototype material is made of sintered authentic stainless steel as well as the referral material but with less carbon presence. Prediction is that material couple does not a significant impact on the friction coefficient.

Work load. The sample was exposed to working condition on durability bench. The temperature during the test was held at a constant value of and $600°C$. The assumption is that the friction coefficient rises rapidly when the sample is exposed to the duty cycle.
.

5.3. Experiment

The experiment was conducted in Garret company test facility. For purpose of this thesis, it was allowed to use a flow bench (figure 5.9), which is in early stages of construction. Controlled variable of the test bench is mass flow. Constant mass flow is secured by actuator which opens and closes the entrance valve. Source of the pressure is secured by a compressor. Fixture is attached to the test by V-bend on one side and to acustic noise filter on the another.

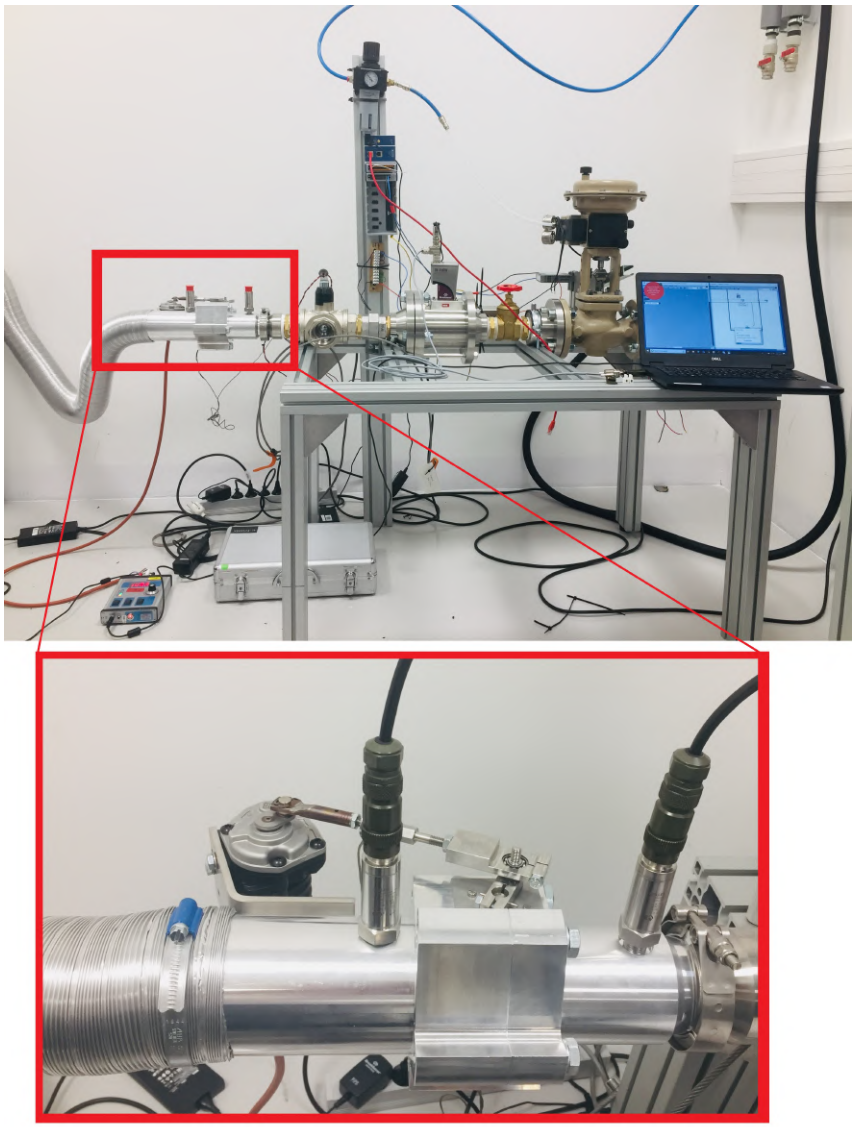

Figure 5.9: Experimental set up

Test of samples composes of sequence of 10 cycles. One cycles includes opening and closing of the valve. As data acquisition unit was used DaQ system by Nation Instrument NI cDAQ-9189. During the test 4 channels were recorded. Sampling frequency was set to 70Hz.

5.4. Output of the experiment

Angle was obtained from an analog position sensor from the actuator. Based on regression, shown in figure 5.5 in chapter 5.1. Movement of the actuator was set, so the valve opens up to 15° and goes back to the closed position. One cycle, from closed to opened and back, was set to 4 seconds. Valve angle development over time is shown in figure5.10. Speed was set lowest as possible although speed needed to be high enough to prevent the stick-slip motion.

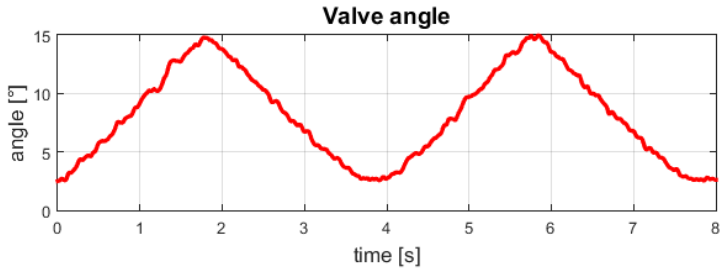

Figure 5.10: Valve channel

As in case of rod force, analog signal was measured from load cell amplifier. Rod force development over time is shown in figure5.11.

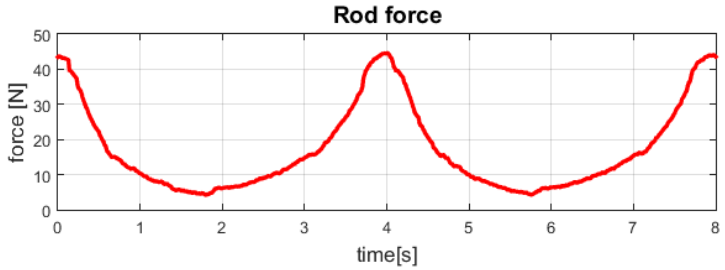

Figure 5.11: Force channel

Pressure on inlet and outlet were calculated based on calibration provided by manufacturer. Each test record were controlled to secure that pressures during the remained same as pressures used as boundaries condition in CFD. Pressure development over time is shown in figure 5.12.

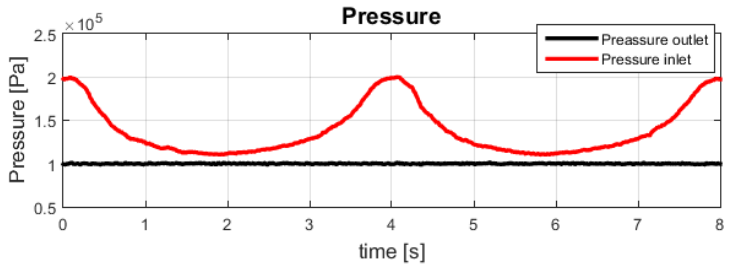

Figure 5.12: Pressure channel

Mass flow was set to constant for all tests to $35g/s$. Therefore this measurement is used only as a control information. Mass flow development over time is shown in figure 5.13.

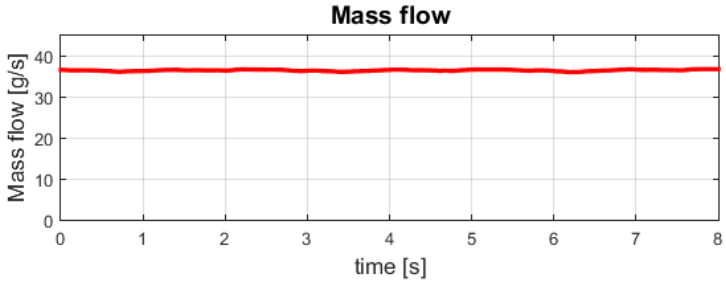

Figure 5.13: Mass flow channel

Pressure on inlet exhibits the hysteresis behavior during the testing. Pressure tends to be lower during the closing in comparison with the opening as seen in figure 5.14.

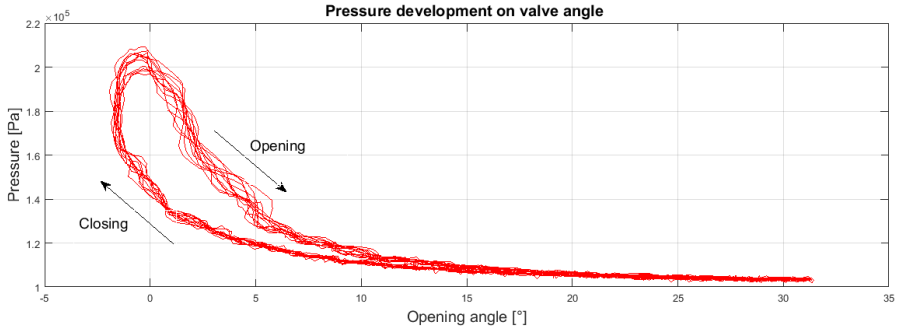

Figure 5.14: Hysteresis of pressure.

This pressure hysteresis causes of switching of opening and closing curves as was presented in chapter 4.5 in figure 4.7. In figure 5.15 can be this effect seen, when valve angle is approximately $15°$. At valve opening angles above $15°$, pressure hysteresis disappears and friction hysteresis becomes noticeable.

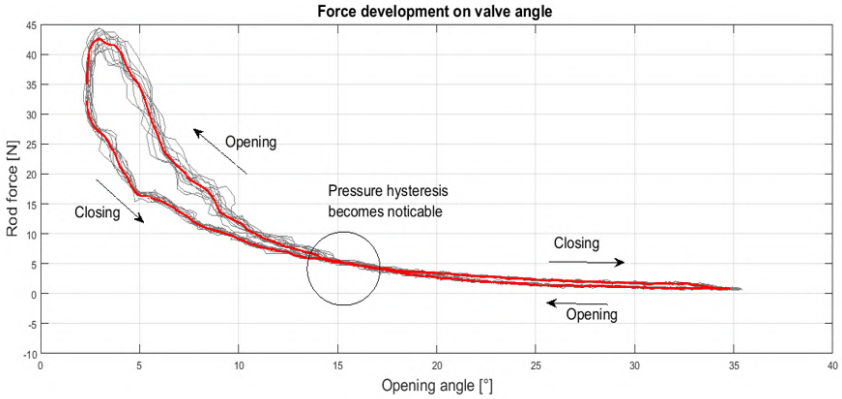

Figure 5.15: Impact of the pressure hysteresis .

Regarding this effect, further evaluation was divided into two cases, opening and closing . The load acting upon the valve has to be computed separately for opening and closing.

At high opening angles, load acting upon the valve becomes insignificant. Therefore, the impact of friction is less recognizable. On the other hand, at valve angles approaching closed position pressure become more unstable. Based on this information, for further evaluation range between 4° and 9° is taken into consideration. One of the most important thing at any testing is repeatability of experiment. In this case the variable that was controlled was pressure. Pressure development of opening and closing must have the same course for all test. In case this demand is not fulfilled, further evaluation would not be possible.

Repeatability was evaluated based on the dependence between valve angle and pressure. Standard error was used as a measure of repeatability. Standard error, in other words, root mean square error, was calculated base on the following equation:

$$e_p = \sqrt{\frac{1}{n}\sum_{n=1}^{i}(\overline{p} - p_i)^2} \tag{5.8}$$

where:

- e_p: standard pressure error
- $\overline{p}_n$: average pressure at given valve angle, calculated from all test.
- p_n: pressure at given angle for specific test.
- n: number of samples.

The standard error between each test and the mean value is $1000Pa$. This value was calculated only for range from which is friction coefficient evaluated, from 4° up to 9°. This low value of standard error testifies about satisfactory repeatability of the experiment.

Average pressure development of all test determines boundary conditions for CFD simulation. Figure 5.16 show boundary conditions for CFD.

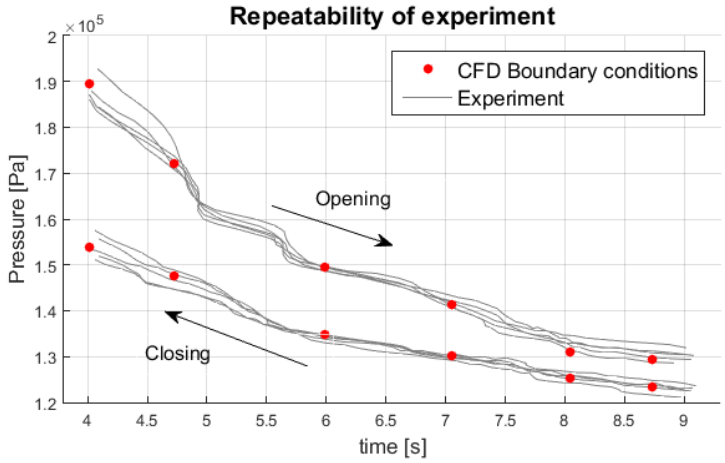

Figure 5.16: Mass flow channel

.

6. Simulation of the environmnet

6.1. Simulation of aero load

Commercial software Ansys was used to compute load that acts upon the valve in the fixture. Ansys is software that solves problems in numerous engineering branches using a numerical method. It finds its use in areas such as statics, thermodynamics, electromagnetic, fluids, and much more. The main advantage of ANSYS is that it reduces time and expenses related to research, which would be otherwise spent on expensive and difficult experiments. As mentioned, ANSYS can be used to compute problems that involve fluid dynamics. The branch that deals with this area is CFD, which stands for Computational Fluid Dynamics. The principle stands on weight conservation law, momentum conservation law, energy conservation law in the form of partial differential equations of Navier-Stokes equation [25].

Ansys provides 2 main features to compute CFD problem, CFX and Fluent. Each feature is suitable for a specific problem. CFX is more preferred for turbo-machinery whereas fluent is more suited for supersonic and hypersonic flows. CFX cannot create a clear 2D mesh. While fluent handles 2D problem with no problems. For purposes of this thesis, the CFX tool was chosen [26].

6.1.1. Setup of the simulation

CFX model consists of one mesh component, which includes the geometry of the fixture and valve and CFX component with pre-processing and post-processing of the simulation. For easier manipulation with the model, opening angle, pressures on inlet and outlet are set at parameters. Figure show layout of the simulation6.1.

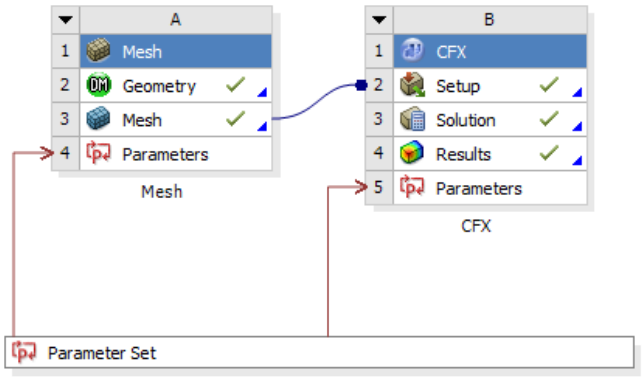

Figure 6.1: CFX layout.

Design points were chosen regarding the experiment. Since pressure dropped rapidly at opening angle 10°, there is no reason to evaluated CFD for angles higher than 10°. On the other hand, pressure and rod force behave unstable at angles near the closed position. Therefore only range between 4° and 9° was evaluated. Six valve angles were selected and evaluated in this range. This means that six design points for opening and six for closing

pressure curve. Boundary conditions, temperature, and pressure on inlet and outlet were obtained from the experiment.

The internal volume of the fixture was modeled in ANSYS DesignModeler based on the model from SolidWork. A simplified model of the valve was modeled in SolidWorks software and exported as a STEP file which was, later on, imported to ANSYS. After the valve was set in place, the opening angle was set by rotating the valve along the shaft axis. Opening angle was selected as a parameter of the simulation. Afterward, the shaft was subtracted from a volume of the fixture. This assembly then represents the negative volume of the fixture.

A local coordinate system (CS) was placed in the axis of the shaft. Origin of CS is located in the contact between bushing and valve. Forces and torques acting upon the valve are evaluated in this CS. Further, in the text, it is referred to this CS a to Valve coordinate system. Valve CS is shown in figure 6.2.

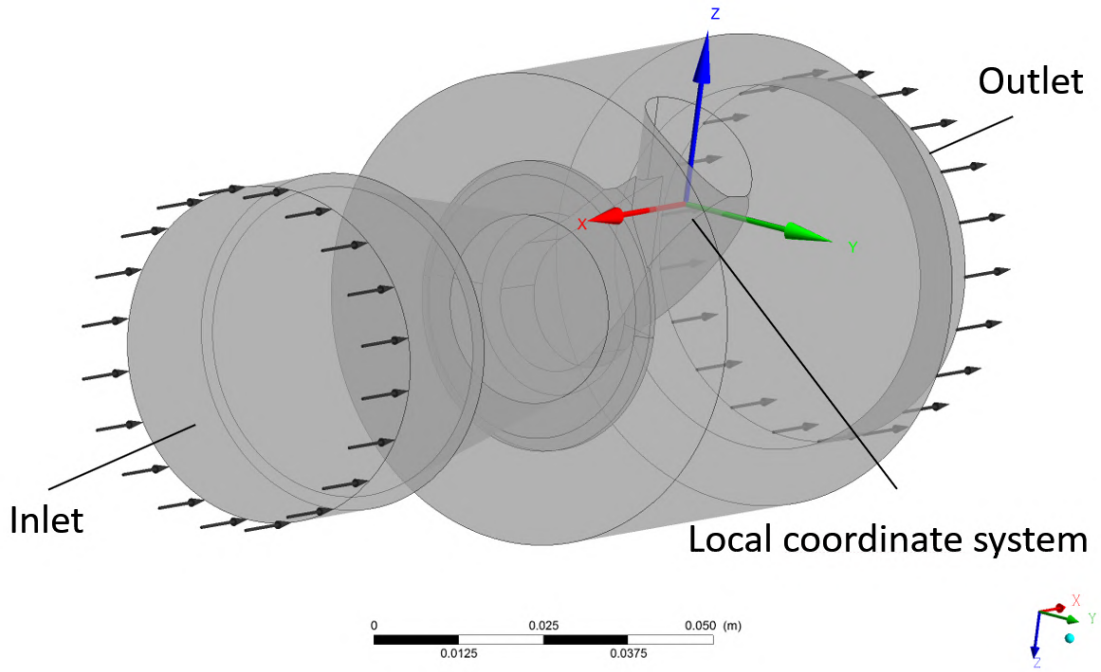

Figure 6.2: CFX setup

Mesh was set as following:

- Maximum size of the body meshing is set to $1.2mm$.
- Mesh around the valve was set finer then the body mesh to maximum value $0.4mm$
- Mesh was edited at the boundary between gas and the fixture by inflation method. The first layer thickness was set to $10\mu m$; the maximum number of the layer was set up to 18 with growth rate 1.18.

Pre-processor stage of the simulation is summarized in the table 6.1.

Boundary conditions were obtained from experiment. All design points are shown in the figure 6.4

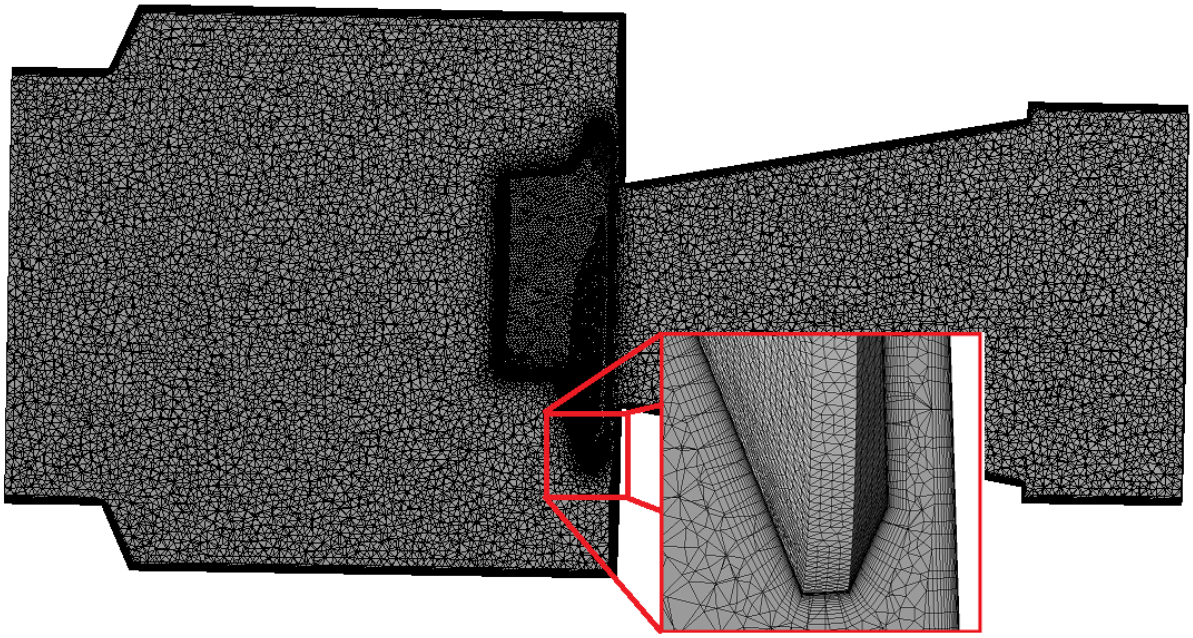

Figure 6.3: Meshing of the model shown in the cross-section of the fixture.

Type of the simulation:	Steady state
Turbulence numeric:	Shear stress transport, first order,medium intensity
Heat transfer:	Total energy
Material:	Ideal gas
Max. iterations:	200
Convergence criteria:	$RMS < 10^{-5}$
Walls:	No slip, Adiabatic heat transfer
Boundaries condition	Input - inlet/outlet pressure,temperature Output - torques/forces on valve

Table 6.1: Preproccesor setup

6.1.2. Results of the simulation

Forces and torques acting upon the valve were evaluated in valve coordinate system described in the previous chapter. Ansys uses expressions to evaluate forces and torques in given CS. Each expression composes of the name of the coordinate system, the axis

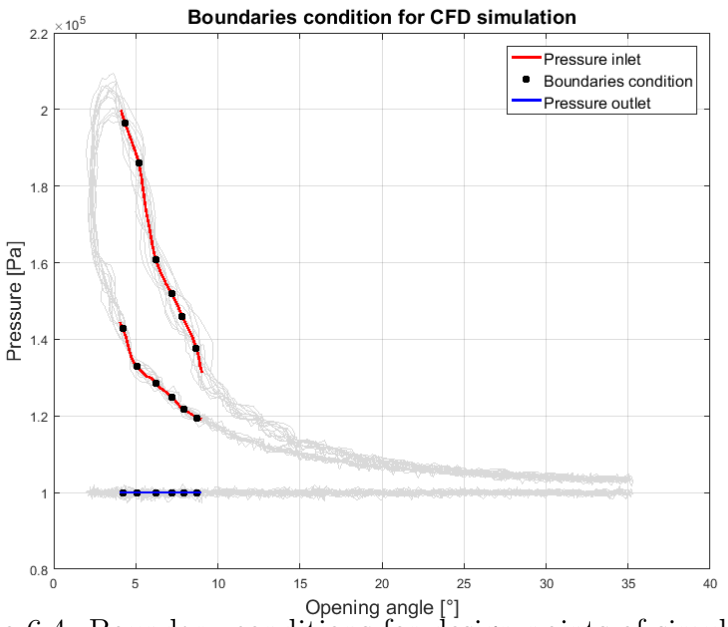

Figure 6.4: Boundary conditions for design points of simulation.

in which a user wants to know a force or a torque and all surfaces of the body. Force is calculated based on pressures applied to surfaces. In this case, expressions are:

$$F_x = \text{force\_x\_ValveCS()@ValveS} \qquad M_x = \text{torque\_x\_ValveCS()@ValveS}$$
$$F_y = \text{force\_y\_ValveCS()@ValveS} \qquad M_y = \text{torque\_x\_ValveCS()@ValveS}$$
$$F_z = \text{force\_z\_ValveCS()@ValveS} \qquad M_z = \text{torque\_x\_ValveCS()@ValveS}$$

Where:

- force or torque are a keywords for ANSYS to evaluate force or torque
- x,y or z specifies an axis
- ValveCS is the name of the coordinate system. If this is left out, Ansys evaluates force/torques in a global coordinate system
- ValveS is a name selection made in the meshing stage. ValveS involves all surface that creates a valve in a fixture.

All design points were able to converge. Control points, forces, and torques in valve coordinate system were stable at the end of each simulation. Results of the simulation are shown in figure 6.5. Components F_y,F_z and M_x had a constant trend close to zero value. Non zero elements,F_x,M_y and M_z , were fitted as exponential curves.

After the first attempt for results, there has been some flaw noticeable on first sight. Forces in In F_y and F_z were constant with an approximate value of $20N$, which in the case of F_z seem very odd. The definition of valve geometry might have caused this. In the first case, the shaft of the valve stands out from the fixture volume. Therefore after subtraction of bodies, the valve in the fixture was represented as a hole in a volume. In the second case, the shaft was shortened to a length smaller the radius of the fixture, which

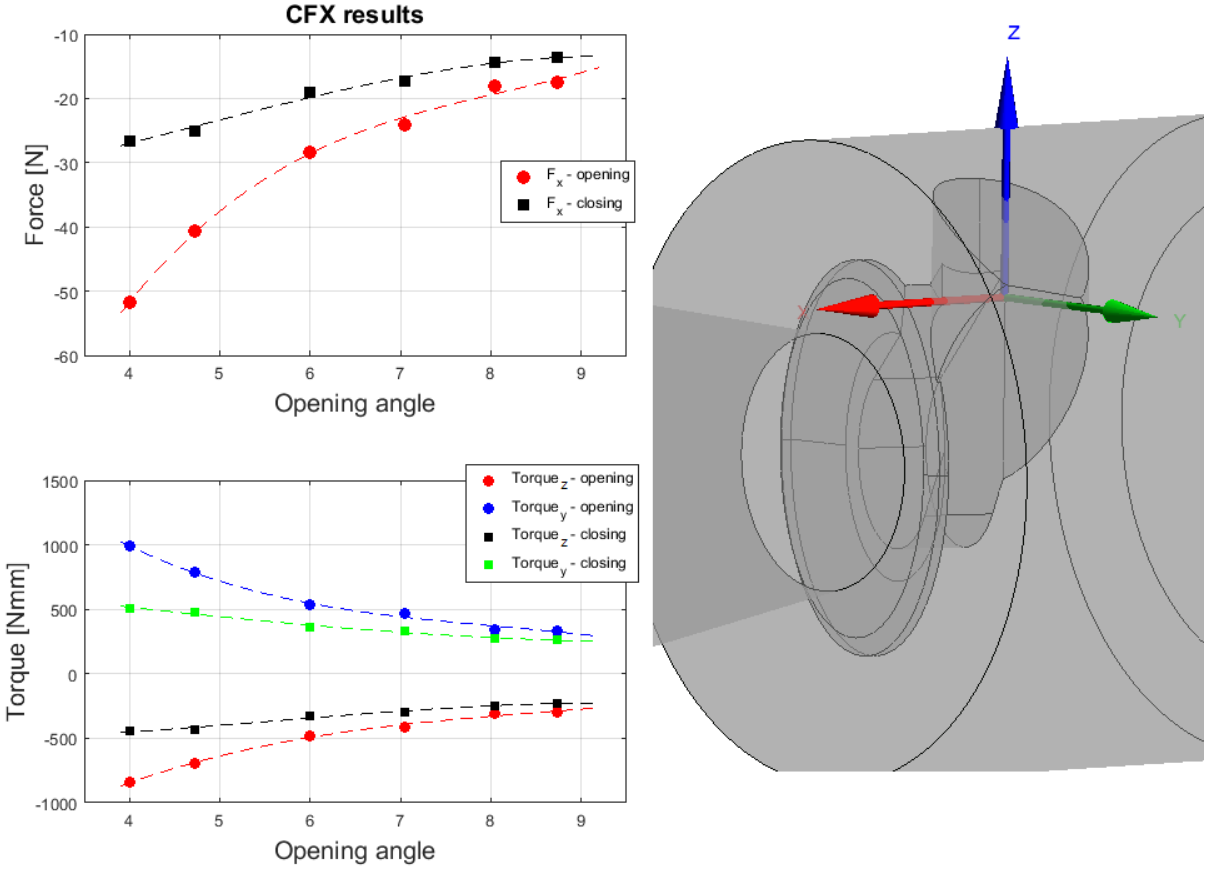

Figure 6.5: Forces and torques development.

results after substation of these two bodies, that the valve in a fixture was represented as cavity instead of a hole. This adjument is shown in figure 6.6.

Most probably, ANSYS evaluated a pressure difference between the certain surface of the valve and outer part of the fixture. Pressure outside the fixture is $0Pa$

After this adjustment force in F_y and F_z dropped nearly to zero. Regarding F_x and M_z and M_y, they remain same with small differences at closed positions $\pm 2N$ or $\pm 5Nmm$. The mentioned adjustment had no impact to flow or pressure development.

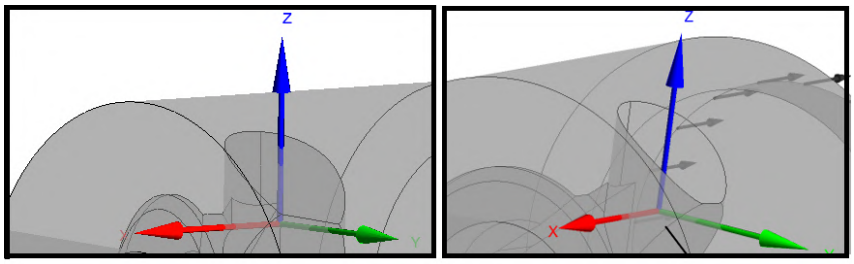

Figure 6.6: Picture on the left displays a situation where valve is represented by hole in the volume. In the left picture is valve represented as cavity.

.

6.2. Simulation of kinematic chain

Simulation of the kinematic chain was conducted in commercial software MSC Adams. This software is of the most used on the field of multi-body systems. Adams finds the primary use in solving kinematic, dynamic, and static problems. Adams is a great tool to study the dynamics of moving part or load and force distribution throughout the mechanical systems. Typical problems are the simulation of the car riding on an uneven road and its impact on the undercarriage, design of the actuating unit, and control system for a various mechanism. One of the powerful features of Adams that it can simulate contact and friction between bodies. This feature can be helpful, for example, for investigating the impact of clearances in systems.

One of the fundamental branches of Adams is Adams view. This software was used to simulate the kinematic chain of the fixture. Picture 6.7 shows the simulation layout.

6.2.1. Adams simulation

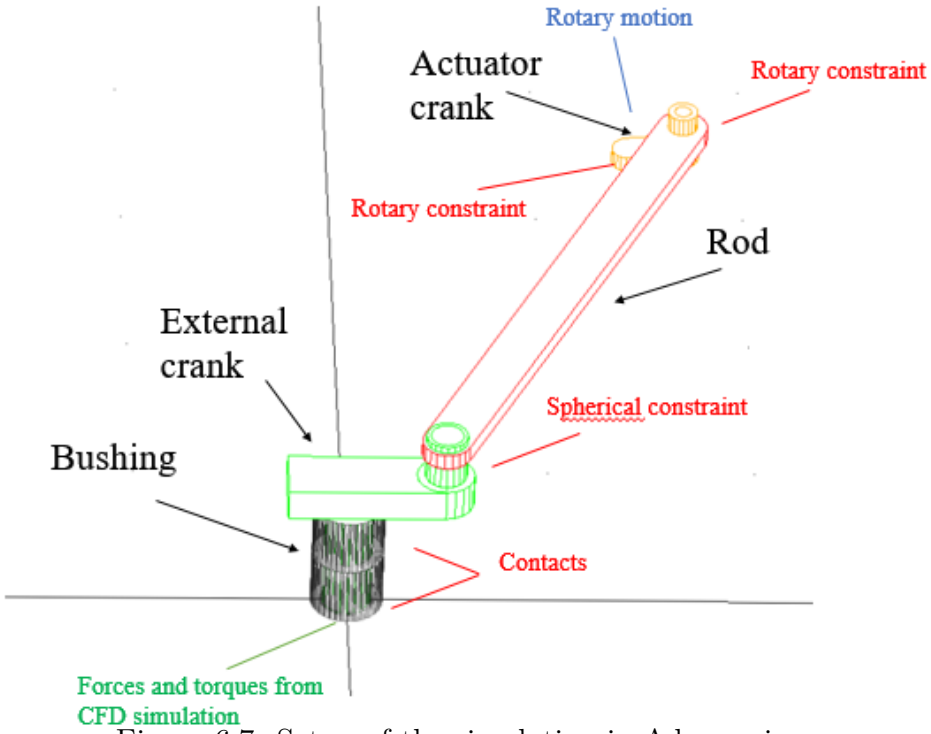

Figure 6.7: Setup of the simulation in Adams view.

Between bushing and shaft was defined contact. There is small clearance between shaft and bushing, therefore shaft slightly tilts in bushing when the load is applied. This cases that 2 contact points occur. One at the top of the bushing and the other on the bottom. For this reason, was bushing divided in half and modeled as 2 bodies added to the ground. Shaft and external crank were modeled as a single body. To the rod is

external crank linked by spherical constraint. Rotary constraints would not allow tilt of the external crank. Rod is linked on the other side to actuator crank by rotary constrain. Actuator crank is linked to the ground by rotary constrain as well. In this last constraint is prescribed actuating motion by the following expression:

$$STEP(time, 0, 0, t_{tol}, \dot{x}) - 2STEP(time, \frac{t_{sim}}{2}, 0, t_{sim}, \dot{x}) \tag{6.1}$$

where:

- t_{tol} - time during which the actuator accelerate to the required velocity
- $\dot{x}$ - angular velocity
- t_{sim} - duration of the simulation

The STEP function approximates the Heaviside step function with a cubic polynomial. This results as rapid acceleration from 0 to angular velocity required $\dot{x}$ in t_{tol} seconds. In half time of the simulation, motion is reversed, by subtracting the same STEP function multiplied by 2.

A force and two torques act at the bottom of the shaft of the valve as seen in figure 6.8 . Force and torques are prescribed as polynomial functions, evaluated from points calculated in CFD. As mention previously, contacts are placed between bushing and shaft. However, one more contact has to be added between crank and bushing. This contact prevents the shaft from floating away.

A measuring object of the valve opening angle is created. This object enables an easier definition of force and torques because the load is not described as a function of time but function of valve angle as it is in case of CFD.

The simulation had problems to converge, and even if, results were not trustworthy. Noticeable peeks in rod force or unstable behavior. The default dynamic solver GSTIFF was changed by WSTIFF, which is less accurate but more stable. Regarding the solver also formulation was change from *i3* to *si2*. Difference between these two is that *i3* has error checking only on position, whereas *si2* includes velocities. *si2* is stable for all time steps. In general can be said that switching from *i3* to *si2* is followed by larger error tolerance [27]. The last measure that was done was that the time step was shortened to 0.001 seconds.

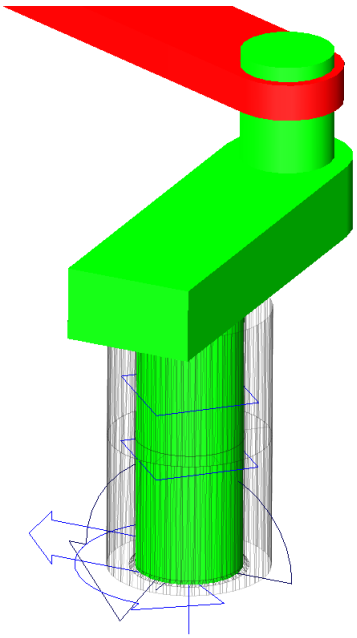

Figure 6.8: Representation of contact

6.2.2. Contact settings

The setting of contact plays a crucial role in the given simulation. The normal force is needed to calculate a friction force between shaft and bushing. There are 2 functions in

Adams that can be used for evaluation of normal force, impact, and restitution. Restitution is not fit for purposes of this simulation; therefore function impact was selected. Impact function launches when the distance between bodies, represented in figure 6.9 by markers I and J, is less than nominal free length, which means that bodies collide. Collision is simulated as a penetration of the body to the another. Impact function can define by the following expression:

$$F_N = \begin{cases} 0 & \text{if } x > x_1 \\ k(x_1 - x)^e - STEP(x, x_1 - d, c_{max}, x_1, 0)\dot{x} & \text{if } x \leq x_1 \end{cases} \tag{6.2}$$

where:

- x - distance between bodies
- x_1 - specific dimension
- $\dot{x}$ - relative velocity of the bodies
- k - Contact stiffness
- e - Force exponent
- c_{max} - Maximum damping
- d - depth of the penetration after which damping remain constant.

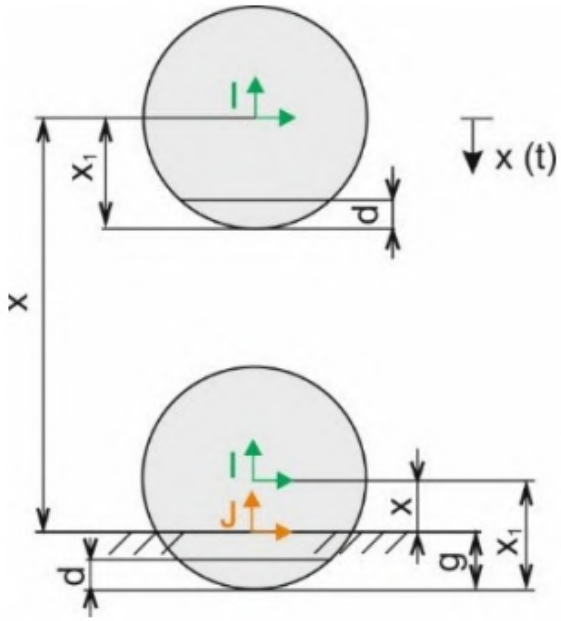

Figure 6.9: Representation of contact

As seen, function impact has 2 force component. First, $k(x_1 - x)^e$ which represent spring or stiffness component and second, the STEP function which represents viscous component or damping. The stiffness results as a resistance against the penetration. Value of the stiffness should be approximately equal to the stiffness of given bodies in the collision. The exponent e causes non-linearity of the spring contact. In general, the exponent can take up values, $e < 0$. For the smoother transition of the spring force when bodies come into the contact, it is better to use $e < 1$. By Adams tutorial tip, for a better run of the model simulation use $e > 2.1$. However, if low penetration is desired, it is better to keep e close to 1. The damping element opposes the direction of the relative motion of given bodies. Function STEP prevents discontinuity when bodies first touch each other. From its definition, is damping function cubic step function. As seen on figure 6.10, after penetration$(x_1 - x)$ reaches certain value (d), damping remains constant.

Setting of the given simulation where set as follows:

Normal force

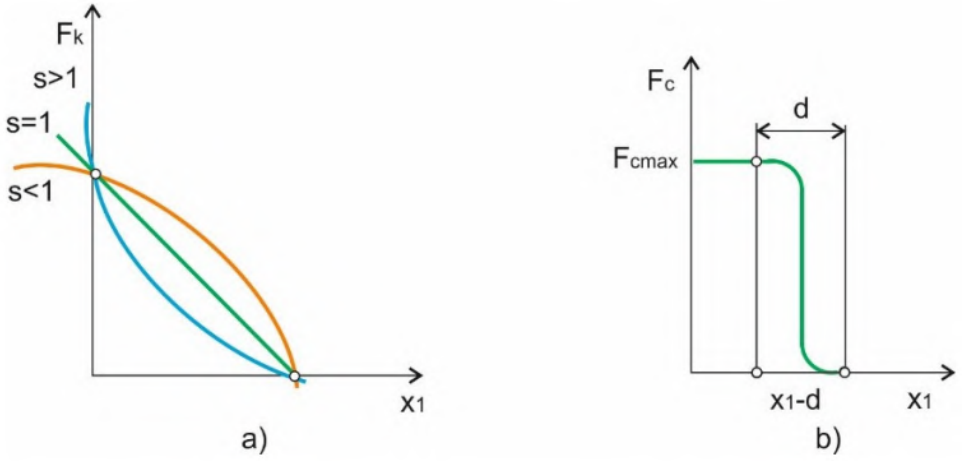

Figure 6.10: a) Exponent e causes non-linear spring b). Damping dependence on the penetration of the bodies

- x - distance between bodies
- x_1 - specific dimension
- $\dot{x}$ - relative velocity of the bodies
- k - Contact stiffness: 10^5
- e - Force exponent: 1.45
- c_{max} - Maximum damping: 100
- d - depth of the penetration: 10^3

Friction force

- v_s - Stiction velocity: 10^{-2}
- v_d - Friction velocity: 0.1

Simulation with default setting was very unstable. Therefore the parameter needed to be tuned. Parameters regarding the friction were explained in chapter 4.3, in which was described Coulomb friction model that Adams implements.

As mention earlier regarding the dynamic solver, One adjustment had been made as well with that part of solver that handles 3D contact operation. The most crucial setting is faceting tolerance. As in the case of ANSYS mesh, faceting is a process of approximating the surface of an object by a mesh of triangles. The default value is set to 300. By increasing this value, the finer mesh is created. Consequently, this increases the computation time and makes the simulation run slower. Recommended range is from 300 to 1000 [23]. In the simulation was faceting tolerance set to 800.

6.2.3. Adams results

The output from Adams was a map rod force developments shown in figure 6.11 . This map includes opening and closing curves for friction coefficients from 0 (No friction) up to 0.9. The figure shows the map of rod forces. Between fiction coefficient 0.1 and 0.2, rod force developments were calculated with step in friction coefficient 0.02. Reason for this was that the expected friction coefficient of brand new samples is between these values. Therefore more precise evaluation is possible. From a given development can be seen that as the friction coefficient increases, flipping of the opening and closing curve, that was described in the chapter 5.3 in the figure 5.15,moves towards the closed position of the valve and at certain point disappears.

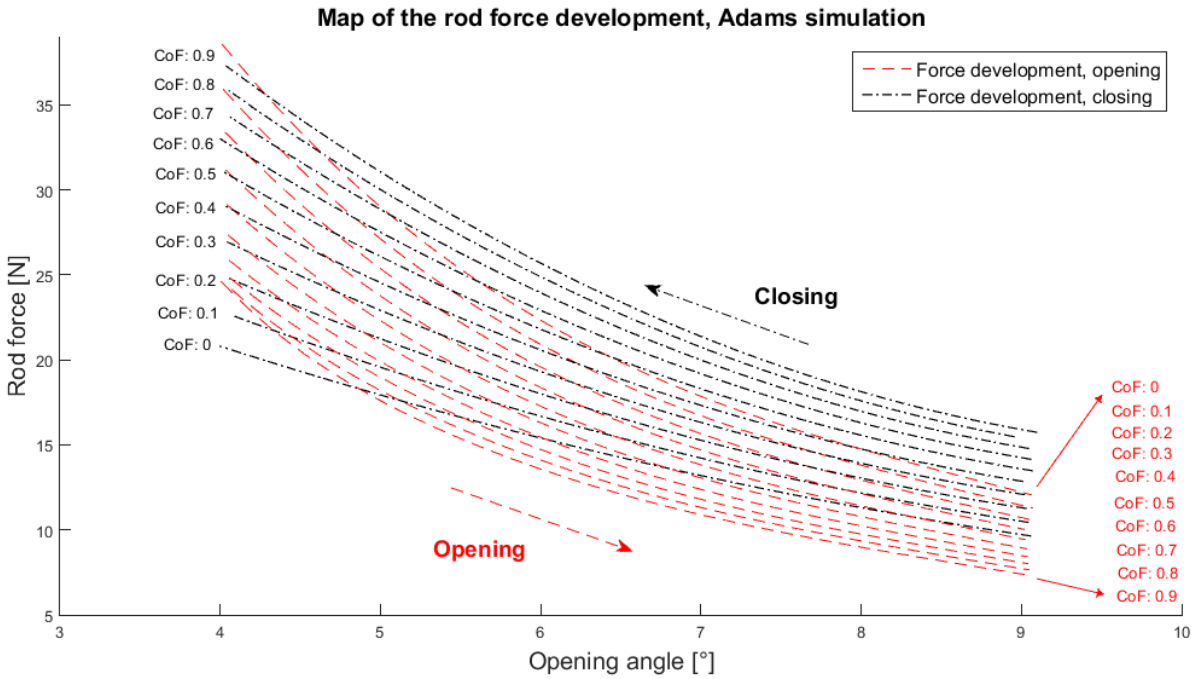

Figure 6.11: The map of force developments for a given motion (opening or closing) and for specific coefficient of friction (Cof).

.

7. Friction coefficient evaluation

In Adams view was created a map of curves shown in the previous chapter. Each curve was calculated for a given friction coefficient. Curves from the test were compared to those from Adams. As a measure for matching of the curves was a root mean square error (RMSE) between experiment curves and curves from Adams. Curves with lowest RMSE were declared as matched. Force curve was obtained as an average of all curves recorded during the test.

As a first sample that was tested was a reference sample. This Sample was used as a base for comparison of other samples. Result of the test and matching of the rod force development can be seen in figure 7.1. The friction coefficient is **0.14**. Standard deviation at matching between Adam simulation was $1.068N$.

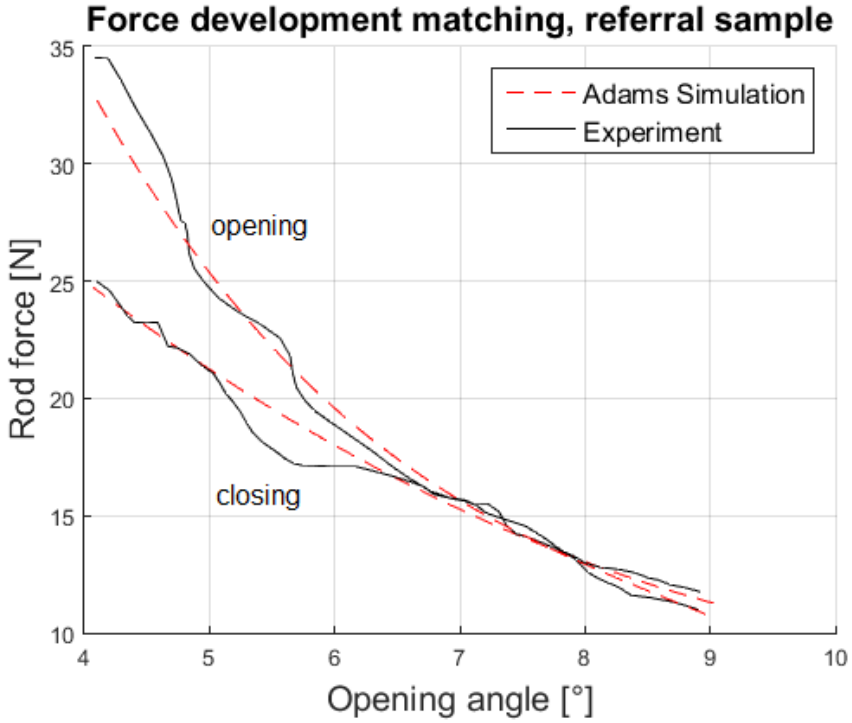

Figure 7.1: Matching of the samples with roughness Ra

7.1. Impact of the roughness

In this case, prototype samples were tested. Their pads are adjusted, so each sample has different roughness. The first sample has a finer surface texture than the referral. Surfaces of the other two samples have higher values of Ra. Sample with polish pads has a friction coefficient of **0.12**. The standard error between Adams simulation and experiment was $0.924N$. Figure 7.2 shows matching of the curves.

Sample with a slightly higher value of Ra than referral exhibits the friction coefficient **0.12** and standard error was equal to $1.014N$. Figure 7.3 shows matching of the curves.

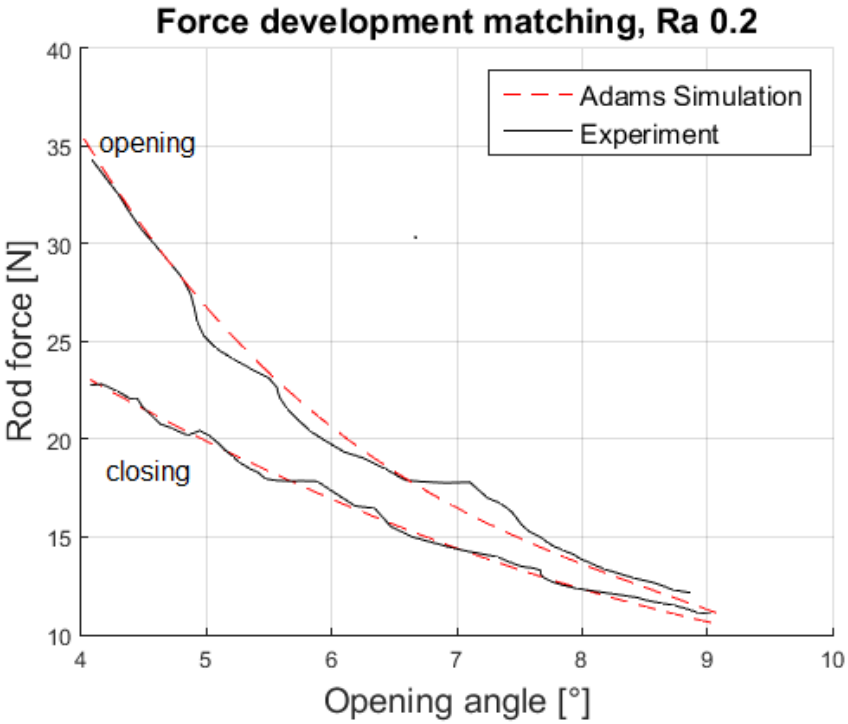

Figure 7.2: Matching of the samples with roughness Ra 0.2

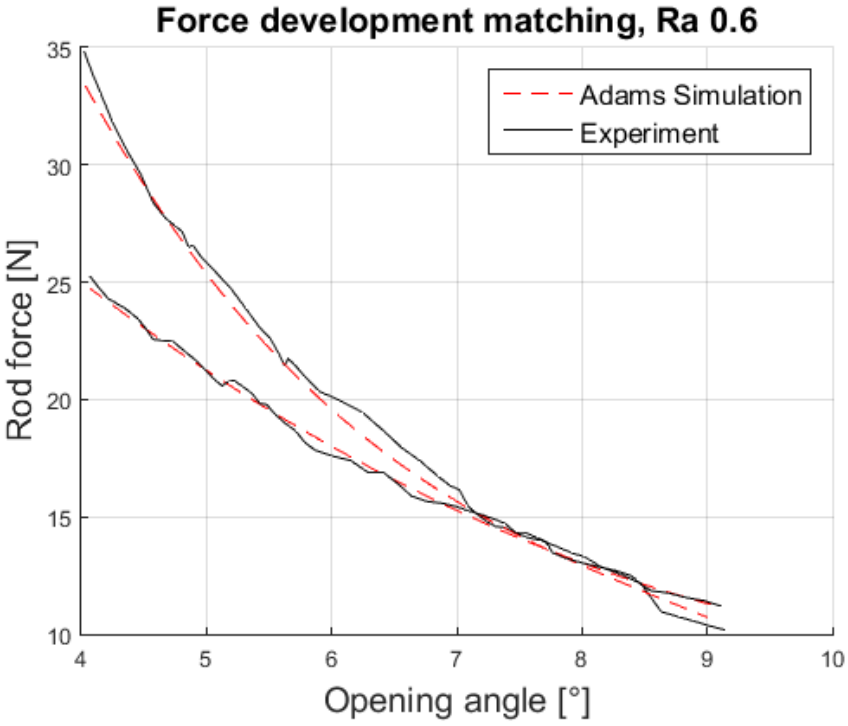

Figure 7.3: Matching of the samples with roughness Ra 0.6

Last of the samples in this section was a prototype with pad roughness Ra 1.2. Error at matching was $0.972N$, and the coefficient of friction is 1.4 Figure 7.4 shows matching of the curves.

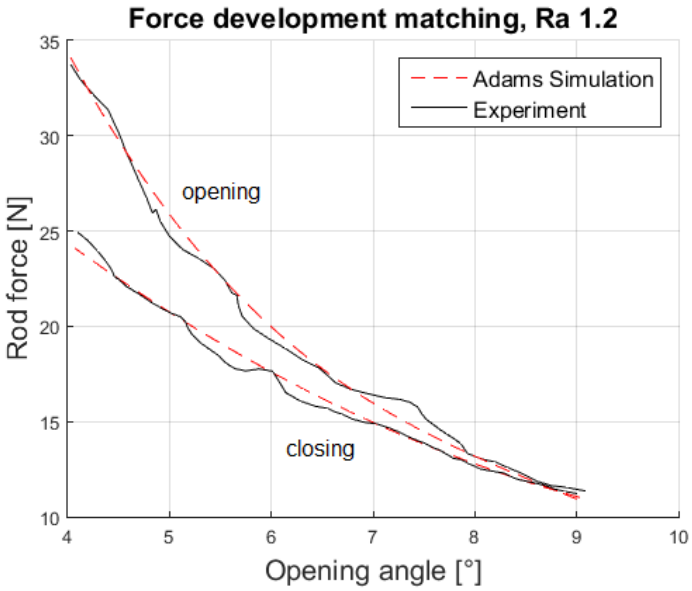

Figure 7.4: Matching of the samples with roughness Ra 1.2

7.2. Material couple

In this case, the reference valve sample was tested with a bushing made of prototype material. The friction coefficient was evaluated as **0.135**. Strand error reached a value of $1.092N$.Figure 7.5 shows matching of the curves.

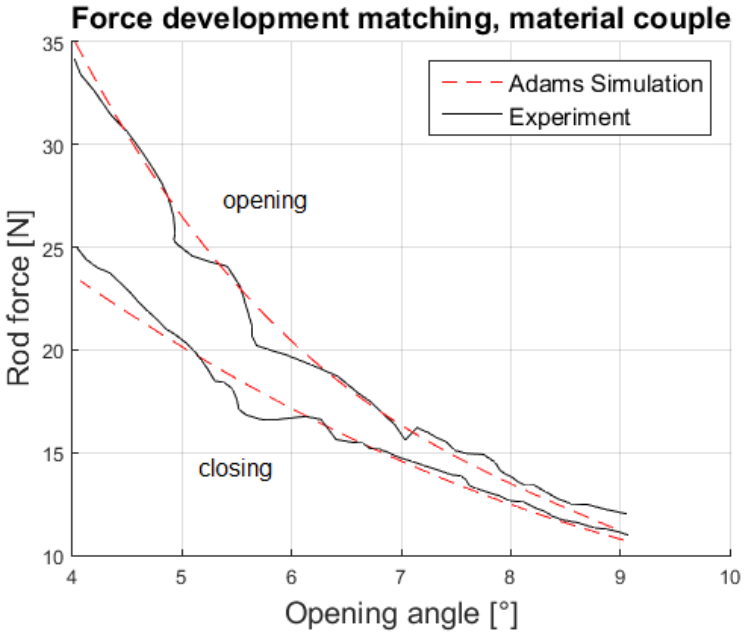

Figure 7.5: Matching of the samples with different material of the bushing

7.3. Wear

Sample undertook a duty cycle at durability test at temperature $600°C$. At durability test, the sample was pre-loaded by a spring and shaft performed 720 000 cycles. The standard error of the matching was $0.899N$. After the duty cycle, the sample exhibits a friction coefficient of 0.69. Matching of the curves can be seen in figure 7.6

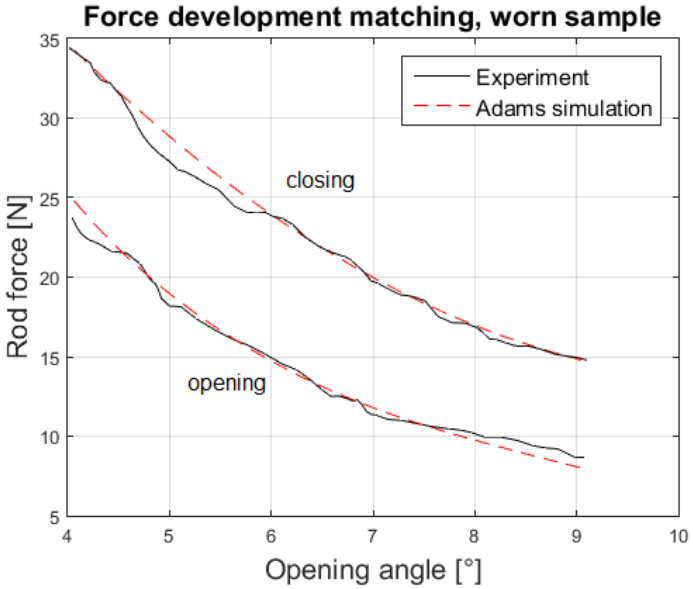

Figure 7.6: Matching of the samples after duty cycle.

Friction at this test was so high, that interception of opening and closing curve occurs right at the closed position. Mention interception is flipping of the curves mention in chapter 5.3 and shown in figure 5.15. The bigger the friction, the interception moves closer to the closed position. At friction coefficient above 0.8, this interception does not occur at all. On first sight, the pressure hysteresis is not noticeable in rod force development.

7.4. Results comparison

For samples with various roughness can be seen a slightly increasing trend of friction coefficient with increasing roughness. This result corresponds with predictions that were before the testing. In case of the surface more than roughness, overall quality of surface has a more significant impact, for example, pollution of the surface or chemical degradation.Comparison of the samples can be seen in figure 7.7

In the case of the sample that undertook duty cycle, worn pads of the valve were rough on visual contact. There were signs after plucked material or holes. Although, the temperature had played a bigger role in such a significant increase in friction coefficient. At first sight, both surfaces, bushing, and shaft were degraded. At high temperatures like that oxides are created on the surface, which is a primary contributor to the friction coefficient. Comparison between new and worn sample is shown in figure 7.8

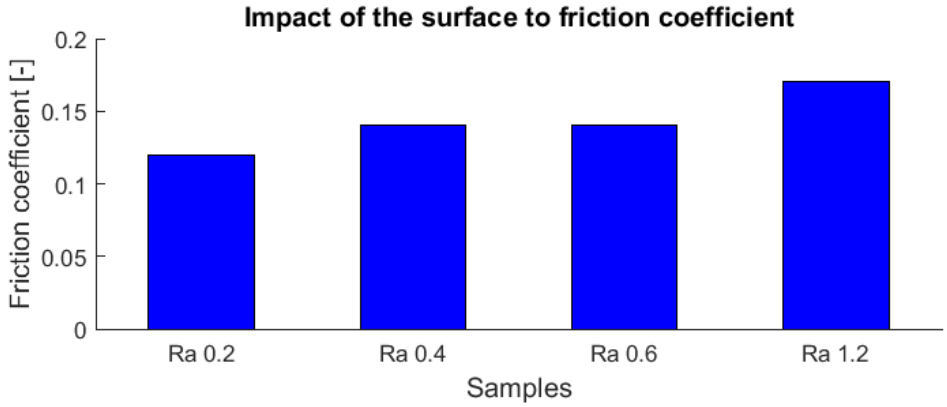

Figure 7.7: Impact of the surface roughness.

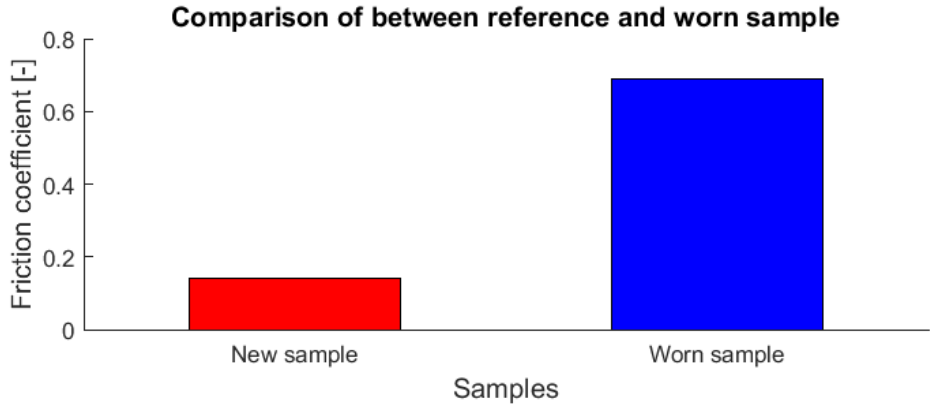

Figure 7.8: Impact of the duty cycle.

Difference between prototype bushing and referral was insignificant. Therefore based on the result can be their friction coefficient declared as coincidence. Comparision can be seen in figure 7.9

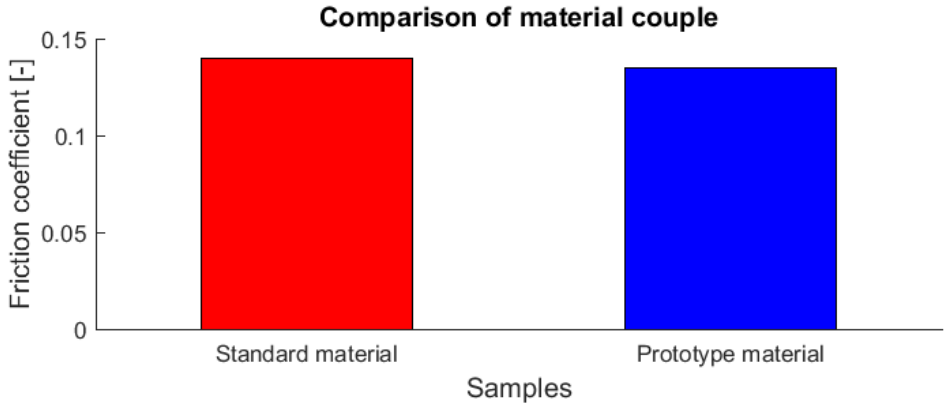

Figure 7.9: Impact of the material couple.

8. Conclusion

The goal of this diploma thesis was to design an experiment method, which would evaluate a friction coefficient in turbocharger's waste-gate system. More specifically between the shaft of the valve and its bushing. At first of all, the test fixture was designed and constructed. The fixture allows testing of a wide variety of valves. The design was developed with high precision and posses many features for proper testing such, as ball bearing connection instead of dry contact in case of shaft crank and rod constrain and many others. Experiment alone arrives as a success with high repeatability. In further sections of this thesis, the aim was set to recreate the test environment by simulation in ANSYS and Adams View. The load applied upon the valve was calculate in ANSYS. CFD simulation provided an authentic recreation of the environment in the fixture during the testing based on boundary conditions from the experiment. Results from ANSYS were used in Adams View simulation. In Adams View was created a model of the four-bar mechanisms which is used to operate with examined valve. This simulation is a credible replica of the real set up. This simulation involves real constraint in the form of contact between shaft and bushing. The output of this model was a force acting upon the rod at given friction coefficient between shaft and bushing. From the development of the forces at the opening and closing movement was created a map which can be seen in figure 6.11 in chapter 6.2.3. Results from the test were plotted against this map to evaluate a friction coefficient for a given system.

Matching of the curves is considered as a success due to the very small standard error of the matching of Adams and experimental rod force development. The friction coefficient of the given samples are reliable and fulfilled expectations and predictions.

There are several upgrades and adjustment that could be done in the future. On a short term basis, there are upgrades regarding fixture. The fixture has 5 other slots at circumference prepared for testing of waste-gate valve with various geometry property. Holes needs to be drilled in these slots for bushings. Also, chamfer the outlet of the fixture and prepare a place for an actuator bracket for each slot.

Regarding the long term basis, more bold upgrades can be made. In chapter 4 were named all factor that has an impact on friction, most of these are related to the nature of the bodies. Although external factors are as important as surface properties. Chapter 3 gave the reader a peak to the working environment of the turbocharger. It is clear that the high temperatures and vibrations play an undeniable role in the friction. Instinctively, the fixture could implement high temperatures. For this adaptation, the fixture could not be made of aluminum as it was in this case. Subsidizing material could be, for example, steel which would raise the weight of the fixture. Another problem which would need to be considered is thermal expansion. As from the perspective of load, the valve system is facing pulsation from an engine piston. This could have bee also included in the consideration. In several studies regarding turbocharger was presented devices that simulated this effect. In Europe, institutions such as Imperial College of London, KTH Royal Institute of Technology (Sweden) or University of Genoa (Italy) has developed such devices that could be implemented to simulated pulsation loading [28],[5],[29].

References

1. TURBOSMART.COM. History of turbocharging. 2011. Available also from: `https://www.turbosmart.com/news/history-of-turbocharging/`.
2. FENSKE, Jason. How Turbocharger Wastegates Work - Internal Vs External. 2016. Available also from: `https://www.youtube.com/watch?v=pn-uCAgB4H8`.
3. ENGINEERS", "INSTITUTION OF MECHANICAL. Innovations in Fuel Economy and Sustainable Road Transport. In: Pune, India: Philadelphia: Woodhead Pub, 2011. ISBN 978-0-85709-213-7.
4. MEDRANO, Maria E. B. *The effect of exit pressure pulsation on the preformance and stability limit of a turbocharger centrifugal compressor*. London, United Kingdom, 2017. Dissertation thesis. Imperial collage London.
5. ROMAGNOLI, Alessandro. *Aerodynamic and thermal characterization of turbocharger turbines: experimental and computational evaluation*. London, United Kingdom, 2010. Dissertation thesis. Imperial collage London.
6. SYSTEMS, BorgWarner Turbo. Design and Function of a Turbocharger. Available also from: `www.turbos.bwauto.com/en/products/default.aspx`.
7. X-ENGINEER.ORG. Variable Geometry Turbocharger. Available also from: `x-engineer.org/automotive-engineering/internal-combustion-engines/`.
8. RAMON, González G. Turbocharger. 2019. Available also from: `drawfolio.com/en/portfolios/ramongarciagonzalez/picture/50173`.
9. HEINRICH, Martin. *Genetic Optimization of Turbomachinery Components using the Volute of a Transonic Centrifugal Compressor as a Case Study*. 2016. Diploma thesis. Technische Universität Bergakademie Freiberg.
10. HATCH, Steve V. Computerized engine controls. In: Clifton Park, NY.: Delmar, Cengage Learning., 2012, vol. 9. ISBN 978-1-1111-3490-7.
11. MOTION, Garrett advancing. Variable Geometry Turbo for Gas Engines. Available also from: `www.garrettmotion.com/turbocharger-technology/gasoline-turbocharger`.
12. HARTZELL. Turbobearings. 2017. Available also from: `hartzell.aero.`.
13. VIVIDRACING. Turbobearings. 2017. Available also from: `vividracing.com/garrett-gt28-gtx28-086-internal-wastegate-turbine-housing-p-152476419.html`.
14. PACPERFORMANCE. Turbosmart WG38 GEN-V ULTRA-GATE 38 external wastegate. 2017. Available also from: `www.pacperformance.com.`.
15. DINH, Khiem. Turbo Tech: Internal vs. External Wastegates. Available also from: `motoiq.com/turbo-tech-internal-vs-external-wastegates`.
16. MOTION, Garrett advancing. Two Stage Serial Turbochargers for Diesel Engines. 2019. Available also from: `https://www.garrettmotion.com/turbocharger-technology/diesel-turbochargers`.
17. DRESEL, Wilfried. Lubricants and Lubrication. In: Germany: Wiley-VCH Verlag GmbH & Co. KGaA, 2017. ISBN 978-3-527-32670-9.

18. BUDINSKI, Kenneth G. Guide to Friction, Wear, and Erosion Testing. In: West Conshohocken, PA.: ASTM International, 2007. ISBN 978-0-8031-4269-5.

19. OBERG, Erick JONES a Franklin D. HORTON. Machinery's Handbook (29th Edition) & Guide to Machinery's Handbook. In: New York,USA.: Industrial Press, 2012. ISBN 978-0-8311-2905-7.

20. TJAHJOWIDODO T., F. AL-BENDER a H. VAN BRUSSEL. Friction identification and compesation in a DC motor. Vol. 38, no. 1. ISSN 14746670. Available from DOI: 10.3182/20050703-6-CZ-1902.00093.

21. PENNESTRI, Ettore et al. Review and comparison of dry friction force models. Vol. 83, no. 3. ISSN 0924-090X. Available from DOI: 10.1007/s11071-015-2485-3.

22. "LIU Y. F. J. LI Z. M. ZHANG X. H. HU, W. J.". Experimental comparison of five friction models on the same test-bed of the micro stick-slip motion system. 2015. ISBN 2191-916X. Available from DOI: 10.5194/ms-6-15-2015.

23. SOFTWARE, MSC. Supplemental Adams Tutorial Kit. In:

24. WANG, Dexin a Yuting RUI. Simulation of the Stick-Slip Friction between Steering Shafts Using ADAMS/PR. Available from DOI: 10.1.1.576.723.

25. ONLINE., CFD. Fluid dynamics. 2013. Available also from: Cfd-online.com.

26. RAGHAV, Raul. Differences between CFX and Fluent. 2007. Available also from: studentcommunity.ansys.com.

27. MADSEN, Jens Bay. Adams Solver Training notes. 2007. Available also from: vehlib.dk/download/Adams_solver_training_notes.pdf.

28. HELLSTROM, Fredrik. *Numerical computations of the unsteady flow in turbochargers.* Stockholm, Sweden, KTH Royal Institute of Technology., 2010. Dissertation thesis.

29. MARELLI, Silvia a Massimo CAPOBIANCO. Steady and pulsating flow efficiency of a waste-gated turbocharger radial flow turbine for automotive application. 2010. Available from DOI: 2010.10.019.

Nomenclature

CFD	Computational fluid dynamics
Cof	Coefficient of friction
DOE	Design of experiment
RMSE	Root mean square error
VNT	Variable nozzle turbine
a, c, l, s	Distance
d	diameter
F	Force in rod
k	Stiffness
M	Torque created by rod force
p	Pressure
r	Kinematic ratio
S	Surface
$\alpha, \beta, \gamma, \delta, \theta$	Angles
μ	Coefficient of friction
μ_d	Coefficient of dynamic friction
μ_s	Coefficient of static friction
$\dot{x}$	Velocity
x	distance
t	time

List of figures